INTERFACIAL AND TRANSPORT PHENOMENA OF BIOINSPIRED VESICLES

by

XIAOLEI CHU

A thesis submitted to the

Graduate School – New Brunswick

Rutgers, The State University of New Jersey

In partial fulfillment of the requirements

For the degree of

Master of Science

Graduate Program in Chemical and Biochemical Engineering

Written under the direction of

Dr. Meenakshi Dutt

And approved by

_____

_____

_____

_____

_____

New Brunswick, New Jersey

May, 2016

ABSTRACT OF THE THESIS

Interfacial and Transport Phenomena of Bioinspired Vesicles

By Xiaolei Chu

Thesis Director:

Dr. Meenakshi Dutt

In the design of drug delivery vehicles, self-assembled nanostructured materials such as liposomes, polymerosomes and hybrid biomaterials bears increasing attentions. The key challenges in the optimal modification of these soft materials is the prediction of resultant morphologies in favor of circulation time, as well as the optimization of surface properties to adjust the interactions between bio-inspired materials with nanoparticles and bio-macromolecules such as peptides, proteins and nucleic acids. One of the ways to overcome these challenges is through the development of flexible modeling tools to address physical phenomena under a mesoscopic scale, allowing us to deeply investigate interfacial problems of nanostructured materials in a dynamic approach. In this work, we utilize the Dissipative Particle Dynamics simulation technique to examine the interaction between peptide mimetic nanoparticles (nanopin) and multicomponent vesicles. We study the role of nanopin architecture and cholesterol concentration on the capture of the nanopins by the bilayer, their insertion and post-insertion self-organization. Furthermore, we investigate the transportation of hybrid vesicle with various concentrations of end-functionalized lipids. We draw correlation among the morphology, composition and mechanical properties of the vesicle and flow conditions. Our results can potentially help

in the design of drug delivery system with respect to their transport in blood capillaries, and tissue engineering for the design of microfluidic devices with better in-vivo transportation efficiency. Our study can also provide guidelines for designing peptide-mimetic nanoparticles or macromolecules which can interface with living cells to serve as sensors for applications in medicine, sustainability and energy.

Acknowledgements

I would like to deliver my deepest gratitude to my advisor Dr. Meenakshi Dutt for the guiding, support and encouragement she has been offering me for the last two and a half years of my graduate study. I joined the Computational Soft Material Group without a slight bit of experience in computational modeling and she taught and trained me with great attention and patience. I truly thank her for digging up opportunities for academic conferences, symposiums and mentoring programs and encouraging me to participate into the communications with other scientists and researchers in the community. It really helped me in developing the skill of delivering my own research. I would like to thank her again for all the efforts she has made in training me to be a qualified scientist.

It is my privilege to have Dr. Roth and Dr. Shapley be my thesis committee members. I want to thank them for accepting my invitation of attending my thesis defense. I owe a deep sense of gratitude to Dr. Roth for helping me resolve the problems I had for credit registration as well as for the inspiring discussion that we once had on the topic of transportation of liposomes in capillary, which literally has evolved into a fantastic project that I have been working on and is included in this thesis. I want to thank Dr. Shapley for offering a wonderful course on Transport phenomena which I found inspiring in the class and even resourceful later when I was engaged with researches that were related with transport problems.

It is my genuine pleasure to work with my fellow colleagues in Dr. Dutt's research group. They are the most helpful peers and we had a wonderful time working, learning and hanging out together. I would like to particularly thank Fikret Aydin as both a mentor and a friend to me for introducing me into computational modeling and helping a lot on several

projects. Fikret taught me with great patience and he never hesitate to help people on good behalf. I am very grateful to have him as my friend. I am extremely thankful to Geetartha Uppaladadium and Srinivas Mushnoori for their great efforts on some collaborative projects with me. I want to thank them for giving enlightening opinions and ideas in the countless discussions that happened in the office.

Last but not the least, I would like to express my gratitude to my family for financially and spiritually supporting me pursuing an advanced degree in the US. I could not have gone so far without them standing behind.

Table of Contents

List of Tables

List of Figures

Chapter 1

Introduction and Objectives

Cell membrane plays a vital role in supporting cell living as an interface that enables mass and energy exchanges between cytoplasm and extracellular solution. The complexity of the surface of a cell enables it to present myriads of kinds of responses and reactions to the contacts from all kinds of molecules and this complexity even varies among types of cells which results into distinct functionalities throughout the body. Apart from the unique mechanical property of lipid membrane, we've recognized that the function of biological sensing is mostly realized via the decorated molecules such as membrane protein, peptide and nucleotides embedded in the lipid membrane. These molecules are in continuous recycling in which inactive molecules are decomposed and new ones are accommodated into the membrane from both inside and outside the cell. Researchers have investigated membrane perturbation induced by Antibacterial peptides (AMP) to fungi, bacterial and even tumor cells.[1-20] The dynamic of perturbation involves insertion of AMPs into the membrane before they start to bind intracellular molecules. Other species of peptide such as Cell-penetration peptide plays important role in transmembrane transportation of big molecules.[21-33] A great potion of both AMP and CPP share common properties of amphiphilicity and charge distribution. Studies have been carried out to combine the traits of CPP and AMP to synthesize peptide with dual effects as both antibiotic and potential drug transporters.[34-37] A promising idea for the design of bio-inspired drug delivery vehicles is through mixing lipid molecules with artificial peptides or proteins to obtain self-assembled nanostructured liposomes with functionalized surface that bear with high

efficiency of bio-recognition and long circulation time. These studies require a fundamental understanding into the mechanism of membrane-peptide interaction and the in-vivo transportation of macromolecules.

One of the major factors that affect the membrane-peptide interaction is the lipid composition of membrane. A good example is that scientists have long found that, unlike with bacterial, typical cationic AMPs exhibit significantly low affinity with mammalian cells.[38] This was then greatly attributed to remarkable compositional differences between eukaryotic and prokaryotic membrane. The membrane of a healthy eukaryotic cell in higher organisms encompasses large fraction of zwitterionic phospholipid and sphingomyelin which result into an electrically-neutral surface property exhibiting lower electrostatic attractions to cationic peptide than negatively charged bacterial surface. This is probably also a partial reason why tumor cells are found to be more sensitive to specific AMPs than healthy cells because the surface of a tumor cell abnormally exhibit unneutralized charge density.[39-40] Cholesterol, which is a small sterol molecule exclusively found in eukaryotic creatures, is believed to be another major factor that inhibits the membrane-disrupting activity of AMPs against eukaryotic membrane.[41-43] Although sterols can also be discovered in some prokaryotic species, none of them have been demonstrated to have membrane-stabilizing functions as cholesterol has to protect the integrity of phospholipid bilayers in eukaryotic entities. The presence of cholesterol in mammalian cell membrane and artificial membrane model have been suggested by a number of studies to reduce antibiotic activities of certain AMPs.[44,45]

The shape of the drug delivery vehicles could also play an important role in determining their properties of in-vivo transportation and bio-recognitions. A study has

shown that due to their morphological characteristics, worm-like micelles circulate longer than the spherical micelles in body.[46] It is reported that a deformable polymer nanosphere is designed to mimic the size and shape of the red blood cell and exhibit improved circulation time and better biodistribution profile. Dobereiner et al.[47] and Sandstrom et al.[48] who worked on mixture of phospholipids, PEGylated lipids and cholesterols discovered morphological transitions of self-assembled structure under different temperatures and with different concentration of cholesterol. These findings show that the shapes of lipid aggregates can be controlled by purposely tuning the composition, which subsequently affect the in-vivo behavior of these structures.

In chapter 2, we introduce a MD-based approach entitled Dissipative Particle Dynamics (DPD), [49-66] which simultaneously resolves both the molecular and continuum scales, and reproduces the hydrodynamic behavior, to examine phase segregation in multi-component lipid vesicles.[51-53,61,62,67,68] Continuum approaches[69-71] have also been used to investigate the phase separation dynamics in mixed membranes.

In chapter 3, we use DPD to simulate the interaction of linear amphiphilic molecules with cell membranes. Systems are built including host cells and individual extracellular molecules to reproduce spontaneous insertion that is observed in some important bio-processes such as the membrane-penetration of CPP and AMP or the embedding of membrane protein as receptors. The host cell is modeled by building a multi-component lipid bilayer vesicle, which is obtained through spontaneous free energy minimization from a preassembled bilayer structure. Previous computational studies have shown that such approach of pre-assembling facilitate the harvest of an intact stable lipid vesicles.[51,61,72-74] A number of other recent studies have investigated the dynamics of self-

assembly from random distributed individual lipids into clusters in structures of bicelles or vesicles.[75-95] In our investigation, we do not focus on the dynamics of lipid self-assembly. Instead, we are more interested in using this bio-inspired lipid vesicle model to mimic peptide-membrane or protein-membrane interactions with linear coarse-grained model herein introduced in this paper with pin-like structure that captures the architecture and amphiphilic properties of some simple peptides and proteins.

In chapter 4, we utilize DPD to investigate the shape characteristics during transport of multicomponent bio-inspired vesicles and sterically stable hybrid carriers through blood vessels that are modeled as cylindrical microfluidic channels. We establish the relation between flow characteristics and shape transition, and further correlate them with variation of mechanical properties such as line tension.

In chapter 5, we make conclusions of our work on the modeling of interfacial and transport phenomena of bioinspired vesicles.

Chapter 2

Modeling lipid molecules using Dissipative Particle Dynamics

2.2 Dissipative Particle Dynamics (DPD)

2.2.1 Technical background

DPD is a mesoscopic MD-based simulation technique that uses soft-sphere coarse-grained (CG) models to capture both the molecular details of the system components and their supramolecular organization while simultaneously resolving the hydrodynamics of the system over extended time scales. [54-57] The dynamics of the soft spheres in the DPD technique is captured through integrating Newton's equation of motion via the use of similar numerical integrators used in other deterministic particle-based simulation methods.[63,96] The force acting on a soft sphere i due to its interactions with a neighboring soft sphere j ($j \neq i$) has three components: a conservative force, a dissipative force and a random force, which operate within a certain cut-off distance r_c from the reference particle i. These forces are pairwise additive and yield the total force acting of particle i, which is given by

$$\mathbf{F}_i = \sum_{j \neq i} \mathbf{F}_{c,ij} + \mathbf{F}_{d,ij} + \mathbf{F}_{r,ij} \tag{2.1}$$

The soft spheres interact via a soft-repulsive force

$$\mathbf{F}_{c,ij} = a_{ij}(1 - r_{ij}/r_c)\hat{\mathbf{r}}_{ij} \quad (\text{for } r_{ij} < r_c) \tag{2.2}$$

$$\mathbf{F}_{c,ij} = 0 \quad (\text{for } r_{ij} \geq r_c) \tag{2.3}$$

a dissipative force

$$\mathbf{F}_{d,ij} = -\gamma \omega^d(r_{ij})(\hat{\mathbf{r}}_{ij} \bullet \mathbf{v}_{ij})\hat{\mathbf{r}}_{ij} \tag{2.4}$$

and a random force

$$\mathbf{F}_{r,ij} = -\sigma\omega^r(r_{ij})\theta_{ij}\hat{\mathbf{r}}_{ij} \tag{2.5}$$

where

$$\omega^d(r) = [w^r(r)]^2 = (1-r)^2 \qquad (\text{for } r < 1) \tag{2.6}$$

$$\omega^d(r) = [w^r(r)]^2 = 0 \qquad (\text{for } r \geq 1) \tag{2.7}$$

$$\sigma^2 = 2\gamma k_B T \tag{2.8}$$

a_{ij} is the maximum repulsion between spheres i and j, $\mathbf{v}_{ij} = \mathbf{v}_i - \mathbf{v}_j$ is the relative velocity of the two spheres, $\mathbf{r}_{ij} = \mathbf{r}_i - \mathbf{r}_j$, $r_{ij} = |\mathbf{r}_i - \mathbf{r}_j|$, $\hat{\mathbf{r}}_{ij} = \mathbf{r}_{ij}/r_{ij}$, $r = r_{ij}/r_c$, γ is viscosity related parameter used in the simulations, σ is the noise amplitude, $\theta_{ij}(t)$ is a randomly fluctuating variable from Gaussian statistics, ω^d and ω^r are the separation dependent weight functions which become zero at distances greater than or equal to the cutoff distance r_c. Each force conserves linear and angular momentum. Since the local momentum is conserved by all of these three forces, even the small systems exhibit hydrodynamic behavior.[63] The constraints imposed on the random and dissipative forces by certain relations ensure that the statistical mechanics of the system conforms to the canonical ensemble.[63,96] The relation between the pair repulsion parameter a_{ij} and the Flory interaction parameter χ for a bead number density $\rho = 3r_c^{-3}$ is given by[63]

$$\chi = (0.286 \pm 0.002)(a_{ij} - a_{ii}) \tag{2.9}$$

2.2.2 Modeling and parameterization of system components

The individual lipid molecules are represented by bead-spring models, in which two consecutive beads in a chain are connected via a bond that is described by the harmonic spring potential

$$E_{bond} = K_{bond}((r-b)/r_c)^2 \quad (2.10)$$

where K_{bond} is the bond constant and b is the equilibrium bond length. In all works included in this thesis, the constants K_{bond} and b are assigned to the values of 64ε and $0.5r_c$, respectively.[54-57] The three-body stiffness potential along the lipid tails has the form

$$E_{angle} = K_{angle}(1+\cos\theta) \quad (2.11)$$

where θ is the angle formed by three adjacent beads. The coefficient K_{angle} is set to be 20ε in our simulations. This stiffness term increases the stability and bending rigidity of the bilayers.[54]

The dissimilarity in the amphiphilic lipid species can arise due to differences in the chemistry of the head or tail groups, which can be modeled effectively through a soft repulsive interaction parameter a_{ij}. Differences in the tail groups can also arise due to molecular chain stiffness that is captured in our model by suitably tuning the hydrophobic tail stiffness parameter K_{angle}.

The soft repulsive pair potential parameters for the lipid molecule head and tail beads were selected to capture its amphiphilic nature. The interaction parameters between the like components, a_{ij}, are based on the property of water.[63] The repulsion parameter between two beads of the same type is set at $a_{ii} = 25$ (measured in units of k_BT/r_c) which is based upon the compressibility of water at room temperature[113] for a bead density of $\rho = 3r_c^{-3}$. The soft repulsive interaction parameter a_{ij} between hydrophobic and hydrophilic beads is set at $a_{ij} = 100\,k_bT/r_c$, and is determined by using the Flory-Huggins interaction parameters, χ, as[63]

$$a_{ij} = a_{ii} + 3.496\chi \quad (\text{for } \rho = 3r_c^{-3}) \tag{2.12}$$

The soft repulsive interaction parameters between the head (h), tail (t) beads of lipid types 1 and 2, and the solvent (s) beads are assigned the following values (in units of k_BT/r_c): a_{ss} = 25, a_{h1h1} = 25, a_{t1t1} = 25, a_{h2h2} = 25, a_{t2t2} = 25, a_{h1t1} = 100, a_{h1s} = 25, a_{t1s} = 100, a_{h2t2} = 100, a_{h2s} = 25, a_{t2s} = 100, a_{h1t2} = 100 and a_{h2t1} = 100. The values of the inter-lipid species head-head a_{h1h2} and tail-tail a_{t1t2} soft repulsive interaction parameters will span values ranging from 26 to 50, to mimic mixtures of lipid species with different head or tail group properties. The soft repulsive interaction parameters are summarized in Table 2.1. These parameters are selected to model the effective distinct chemistry of the molecular species, thereby capturing the differences in the melting temperature of the individual species.[49-66] This approach enables us to develop a simple representation of mixtures composed of lipids with two hydrocarbon tails.

In our simulations, the respective characteristic length scale and energy scale are r_c and k_BT. As a result, our characteristic time scale can be described as

$$\tau = \sqrt{mr_c^{\,2} / k_BT} \tag{2.13}$$

Finally, σ = 3 and $\Delta t = 0.02\tau$ are used in the simulations along with the total bead number density of $\rho = 3r_c^{-3}$ and a dimensionless value of r_c = 1.[55] The mass of all the beads is set to unity.[49-66]

2.2.3 Length, time and energy scales of the system

We draw a correspondence between our model and physical systems via the experimental properties of biological lipid bilayers. We obtain the characteristic length scale for our model through the comparison of experimental measurements of the

interfacial area per lipid of a DPPC bilayer with similar measurements from our simulations. Experimental measurements of the area per lipid of DPPC bilayers were found to be 64 A^2 at 50 ^oC.[97] To compute the average area per lipid, the vesicle is divided into 128 rectangular patches with an average area of 10.5 r_c^2 so that each patch can be treated as a bilayer membrane. The average area per lipid for the vesicle bilayer is computed by summing the areas of all the patches, and averaging over the total number of lipid molecules in all the patches. Using the value for the area per lipid (1.12 r_c^2) computed for a stable self-assembled single component lipid vesicle, the length scale for our model is r_c = 0.76 nm.

The time scale τ was calculated to be 6.0 ns by comparing the experimental measurement of the diffusion coefficient of dipalmitoylphosphatidylcholine (DPPC) bilayer, which is given by $5x10^{-12}$ m^2/s,[60] with that obtained from the simulations. The diffusion coefficient of the lipid molecule in the simulations can be found by tracking the mean squared displacements of 10 lipid molecules in a vesicle bilayer. We use the relation

$$\frac{\partial \langle r^2(t) \rangle}{\partial t} = 2dD \tag{2.14}$$

to relate the diffusion coefficient D to the mean square displacement of a particle in a time interval t. The variable d is the dimensionality of the system that is given to be 3 for our system. We calculate the diffusion coefficient D to be 0.052 r_c^2 / τ, using the slope of the time evolution of the mean square displacement. Using a temperature of 50 ^oC, the energy scale is calculated to be $\varepsilon = k_BT = 4.5x10^{-21}$ J.

Chapter 3

Modeling Interactions between Multicomponent Vesicles and Anti-Microbial Peptide Mimetic Nanoparticles

3.1 General overview on interaction of lipid bilayer with nanoparticles

The interaction between peptides, proteins or macromolecules with cell membranes underlie many natural and synthetic processes such as the signal transduction, blood coagulation cascade, drug delivery, sensing or disruption of microbial membranes. The amphiphilic nature of these molecules enables them to bind to the membrane, and potentially induce changes significant enough to influence the structure and function of the cell membrane. For example, amphiphilic antineoplastic agents such as vinblastine and chlorpromazine are found to destabilize the membrane at high concentrations through drug-membrane interactions.[99,100] Another example is the interfacial adsorption of critical concentrations of antimicrobial peptides onto bacterial membranes, their insertion and self-organization into transmembrane pores or channels which have been shown to be cytotoxic.[101-103] The peptides can inspire the design of nanoparticles with controlled spatial organization within the cell membrane following its capture and insertion into the bilayer, for applications involving cellular sensing or stimulation for proliferation and growth. The nanoparticles or rod-coil macromolecules can be synthesized to encompass a rigid hydrophobic aromatic chain or an α helix, with a chain-like hydrophilic functional group.[104-106] A fundamental understanding of the factors driving the binding, insertion and spatial distribution of various amphiphilic macromolecules, or nanoparticles will support

the development of bionanomaterials for functional integration with cells via interfacial binding.

Experimental approaches have been employed to synthesize peptide-mimetic nanoparticles.[107-112] Arylamide oligomers are amphiphilic amino-acid based polymers with a stiff backbone compared to AMPs, and thus are reported to have higher antibacterial activity than typical AMPs such as maganin.[109,111] Nonpeptidic polymeric molecules such as phenylene ethynylenes and polyguanidinium oxanorbornene are reported to form oligomers that adopt amphiphilic and rigid structures in the membrane environment and exhibit strong antimicrobial activity.[108,110] A recent study utilized functional building blocks of peptides, polymers and pH-responsive moieties to design hybrid amphiphilic macromolecules which adopt pin-like structures and exhibit selective cytotoxicity against tumor cells.[112] However, the resolution of experimental techniques limits the identification of the fundamental mechanisms underlying the interaction between the peptide mimics and the cell membrane at the nanoscale. A fundamental understanding of the mechanisms underlying the interaction between the peptide mimics and the cell membrane can guide and refine the design of the mimics for specific functions. The mimic-membrane interactions are dependent upon complex biological processes that involve multiple factors such as the size of the particle, hydrophobic mismatch, electrostatic interaction, membrane composition and physiochemical conditions of the environment (that is, temperature and pH).[104,113-117] Computational techniques can be employed to identify the underlying mechanisms and factors controlling the interactions of amphiphilic macromolecules or nanoparticles with the cell membrane. All-atom simulations of lipid bilayers can resolve the dynamics and structure of various molecules but limit the investigation to small spatio-

temporal scales.[118-124] These tools are not suitable for addressing phenomena occurring on the mesoscale, such as membrane fusion and rupture, domain formation in multicomponent membranes as well as the structural and dynamical effects of nanoparticle adsorption, insertion and self-organization in the membrane.[125] Dynamical processes spanning large length and time scales can be resolved via coarse-grained implicit solvent models which are used along with Monte Carlo,[126-128] Molecular Dynamics (MD),[124,129,130] Brownian dynamics simulation methods[131,132] or mean field theoretical approaches.[133-138]

Earlier studies of the interactions between nanoparticles and biomembranes have used multiple computational techniques.[139-145] We have adopted the MD-based simulation technique entitled Dissipative Particle Dynamics (DPD)[139,146-148] which simultaneously resolves both the molecular and continuum scales as well as the hydrodynamics of the system. The DPD method has been used to investigate the dynamics and morphology of self-assembly, phase separation and phase transition in lipid-based systems,[70,144] block co-polymers,[145,146] dense colloidal suspensions,[147] polymers in dilute solution or in a melt[148] and chains in microfluidic channels.[149,150] The technique has also been used to study the translocation process of the nanoparticles across lipid vesicles[151] and membranes,[152,153] and the different pathways of spontaneous nanoparticle penetration into a vesicle[154] and examine spontaneous insertion of amphiphilic nanotubes into a lipid vesicle and membrane, and their organization in the bilayer.[56,57] We provide a more detailed description of the DPD simulation technique in the Methodology section.

In this work, we study the interaction of peptide-mimetic nanoparticles or nanopins with model lipid bilayers. These nanostructures can be simplified representations of membrane-active peptides and nanoparticles, including tilted peptides, AMPs, surfactant-

like peptides, amphiphilic drugs and rod-coil macromolecules.[101-111,155-159] We are interested in investigating the dynamics and driving force of binding, self-organization and orientation of the surfactant-like nanoparticles, or nanopins, during their interaction with membrane. Our results can potentially guide the design of nanoscale sensors or probes to interface with living cells for applications in medicine, energy or sustainability.

3.2 Modeling and parameterization of system components

We model a ternary vesicle encompassing two distinct amphiphilic phospholipid species, 1,2-dipalmitoyl-sn-glycero-3-phosphocholine (DPPC) and 1,2-dimyristoyl-sn-glycero-3-phosphocholine (DMPC), and cholesterol, as respectively shown in Fig. 1 (a), (b) and (c). The dissimilarity in the amphiphilic lipid species can arise due to differences in the chemistry of the head or tail groups, which can be modeled effectively through a soft repulsive interaction parameter a_{ij}.[160] The two lipid species are represented by bead-spring models, and are modeled by a head group comprised of three hydrophilic beads and two hydrocarbon tails represented by three hydrophobic beads each. The cholesterol molecule is modeled by a head group comprising of two hydrophilic beads and a single hydrocarbon tail encompassing seven hydrophobic beads.

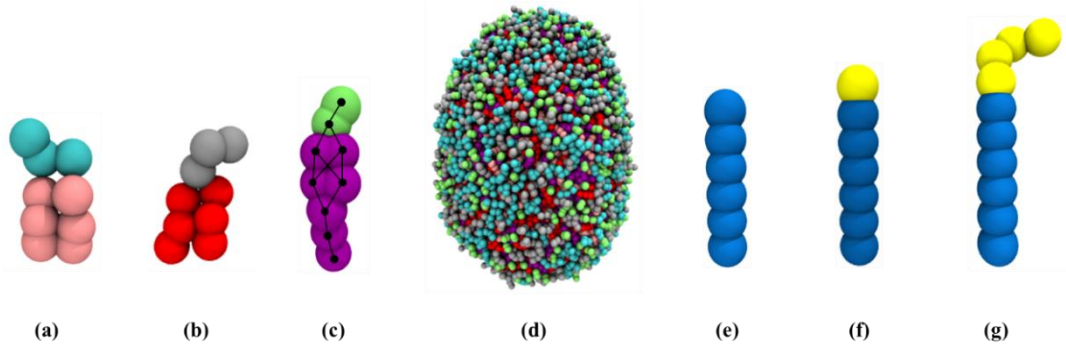

Figure 3.1 Image of coarse-grained model for (a) DPPC, (b) DMPC, (c) Cholesterol, (d) ternary vesicle encompassing 767 DPPC, 767 DMPC and 767 cholesterol molecules, (e) Nanopin H0, (f) Nanopin H1 and (g) Nanopin H4.

To effectively model the rigidity of the cholesterol molecule, additional bonds linking the diagonal pairs of beads are introduced within the ring moiety of the cholesterol molecule, as shown in Fig. 1 (c). These additional bonds are responsible for the difference in the stiffness between phospholipid and cholesterol molecules. As a consequence, the concentration of cholesterol will impact the fluidity of the bilayer by decreasing the average area per lipid.[161]

We draw inspiration from linear α-helical antimicrobial peptides (AMPs) and model the amphiphilic macromolecules by pin-like structures, or nanopins. Experimental counterparts of the nanopins include synthetic AMP mimetics such as Arylamide Oligomers, poly(phenyleneethynylene), polynorbornene and rod-coil molecules.[101-110] We focus our investigations on short nanopins to understand their capture by the bilayer, their insertion, orientation and spatial organization in the vesicle bilayer, and their possible translocation across the bilayer.[54-57,161] Our results can be extrapolated to provide insight into experimental observations on the interactions between synthetic amphiphilic macromolecules or AMPs with cell membranes.[113-117,160,161] The nanopin is modeled by a rigid rod composed of 6 hydrophobic beads with a spacing of 0.5 r_c between the centers of mass of two consecutive beads. The length of the hydrophilic segment serves to regulate the overall hydrophobicity of the nanopins, and is designed to be flexible for one of the nanopin architectures. We consider three nanopin architectures: HN is a pure hydrophobic rigid rod with 6 beads; H1 has the same architecture as HN but with a hydrophilic bead at one of the ends of the hydrophobic rigid rod, and H4 is comprised of a tether encompassing three hydrophilic beads which are attached to the hydrophilic bead in H1, as shown in Fig 3.1 (e) – (g).

The soft repulsive interaction parameters a_{ij} between the head (h), tail (t) beads of DPPC, DMPC, cholesterol, nanopins and the solvent (s) beads are given by a_{hh} = 25, a_{ht} = 100, a_{hs} = 25, a_{tt} = 25, a_{ts} = 100 and a_{ss} = 25. The interaction parameter between cholesterol head beads and solvent beads is set to be a_{hs} = 15, due to the stronger affinity of the cholesterol hydroxyl head group with water molecules. These parameters are selected to model the effective distinct chemistry of the molecular species, thereby capturing the differences in the melting temperature of the individual species.[51,62,75,144] This approach enables us to develop a simple representation of a multicomponent vesicle bilayer encompassing different amphiphilic species.

3.3 Results and discussion

3.3.1 Aggregation of Nanopins in solution

We begin with a preassembled ternary vesicle encompassing a 1:1:1 mixture of DPPC, DMPC and cholesterol, as shown in Fig 3.1(d), in a simulation box of dimensions 50 r_c x 50 r_c x 50 r_c. The simulation box has periodic boundaries along the three axes, with a total of 2301 phospholipids and cholesterol molecules. The total number of beads in the system (including the solvent beads) is 375,000. The phospholipid and cholesterol molecules are spatially arranged in the vesicle bilayer such that the hydrophilic head groups are exposed to the aqueous environment on both sides of the bilayer, and the hydrophobic tails lie in the core of the bilayer. We run the simulation for a time interval of 30,000 τ, and monitor the total energy to check for equilibration. We introduce 10 H4 nanopins into the simulation box such that they are outside the interaction range from each other and the vesicle surface. The total number of beads in the simulation box is kept constant by replacing the corresponding number of solvent beads with nanopin beads. The simulation

is run until all the nanopins have been inserted into the vesicle bilayer. The system is allowed to equilibrate for an interval of 30,000 τ before the next 10 H4 nanopins are introduced into the simulation box using an identical protocol. We repeat this process until 80 nanopins are inserted in the vesicle bilayer. We examine the mechanisms underlying the interaction between the nanopins and the vesicle; the orientation and organization of the nanopins in the bilayer and the role of cholesterol. We adopt the same protocol for the other nanopin architectures (HN, H1). The characterization for each system uses particle trajectories from four simulations that have identical initial positions but different initial velocities and random seeds.

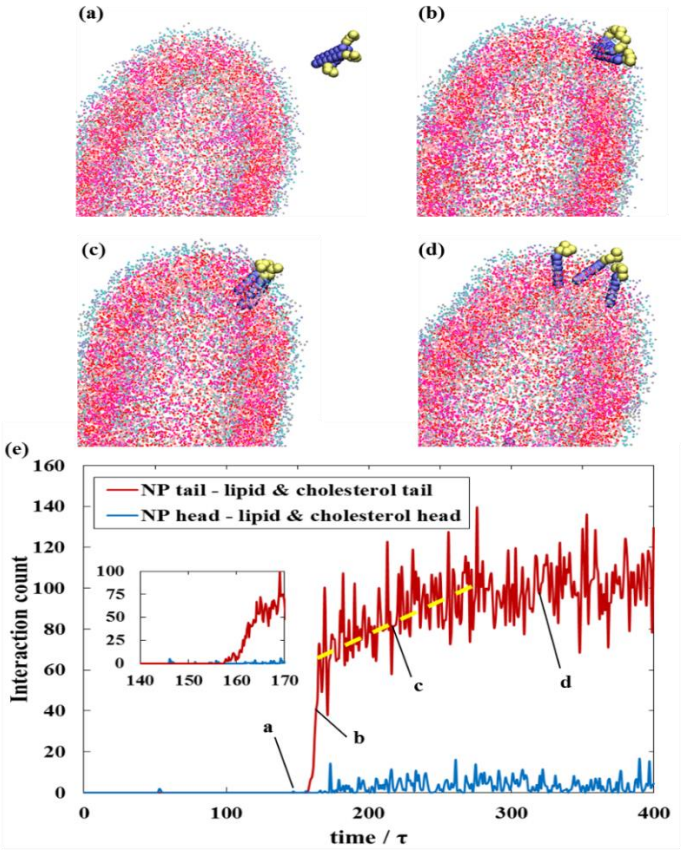

Figure 3.2 (a-d) Snapshot of system with 10 NPs and 2301 lipid and cholesterol molecules, with 3 nanopins at time (a) t = 150 τ, (b) t = 160 τ, (c) t = 225 τ, and (d) t = 340 τ. (e) Time evolution of the interaction count between tail groups of inserted nanopins and membrane components, and between head groups of inserted nanopins and membrane components.

At earlier times, the unfavorable enthalpic interactions between the hydrophilic solvent and the hydrophobic segments of the nanopins promote the self-assembly of the latter, as shown in Fig 3.2 (a). The size of the aggregates can range from two to four nanopins, for a set of 10 nanopins introduced into the simulation box. The nanopin aggregates adopt bundle-like structures where the rigid hydrophobic rods are aligned parallel or anti-parallel to one another, as shown in Fig 3.3. The H4 nanopins adopt orientations that minimize the free energy of the system by maximizing the tether conformational and solvent configurational entropy. Hence, the hydrophilic tethers of the H4 nanopins assembled in a bundle will orient themselves away from each other. We would like to the note that the self-assembly of acetylated AMPs in aqueous medium prior to the incipience of peptide-membrane interactions has been reported in experiments.[162-164] The AMP aggregates have been posited to be responsible for increased cell-selective toxicity, in comparison to their monomer counterparts.[162,163]

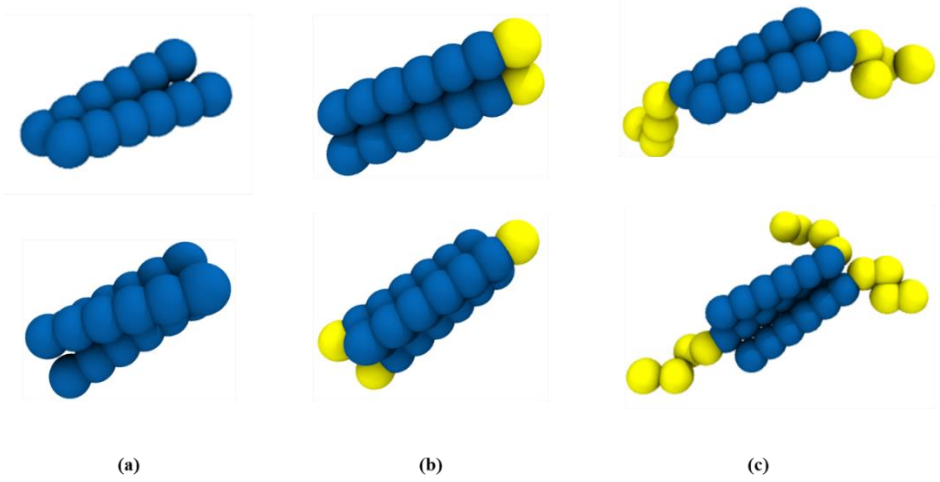

Figure 3.3 Cluster configurations for nanopins of architecture (a) H0, (b) H1, (c) H4.

3.3.2 Spontanous insertion and spatial organization of nanopins in vesicle

Following the aggregation of nanopins in the solution, we observe their spontaneous binding to the vesicle bilayer, as shown in Fig 3.2 (b). We observe the binding events to be initiated by interactions between the hydrophobic components of the nanopins and the bilayer. This observation gives rise to a hyphothesis that the unfavorable enthalpic interactions between the hydrophobic components of the nanopins and the hydrophilic solvent drive the spontaneous capture of the nanopins by the vesicle bilayer and their subsequent insertion into the bilayer. To test this hypothesis, we investigate the insertion of a single H4 nanopin aggregate by examining the time evolution of the interaction count between hydrophilic and hydrophobic components of the phospholipids, cholesterol molecules and the nanopins. A pair of beads is considered to be interacting if their center-to-center distance is smaller than the interaction cut-off distance. The initial binding of an aggregate to the bilayer is characterized by the rapid increase in the interaction count between the hydrophobic components of the bilayer and the nanopins in comparison to that for the hydrophilic components (see Fig 3.2 (e)), thereby supporting the hypothesis. The slower increase in the interaction count between the hydrophobic components (spanning the time interval of 115 τ) indicates the disassembly of the nanopin aggregate accompanied by the diffusion of the individual nanopins in the vesicle bilayer, as shown in Figs 3.2 (c) and (d). The interaction count between the hydrophobic components increases until the aggregate has completely disassembled and all the nanopins are outside the interaction range from each other. We surmise that the disassembly of the nanopins is driven by the

minimization in the free energy by increasing the conformational entropy of the hydrophilic chains and the orientational entropy of the nanopins.

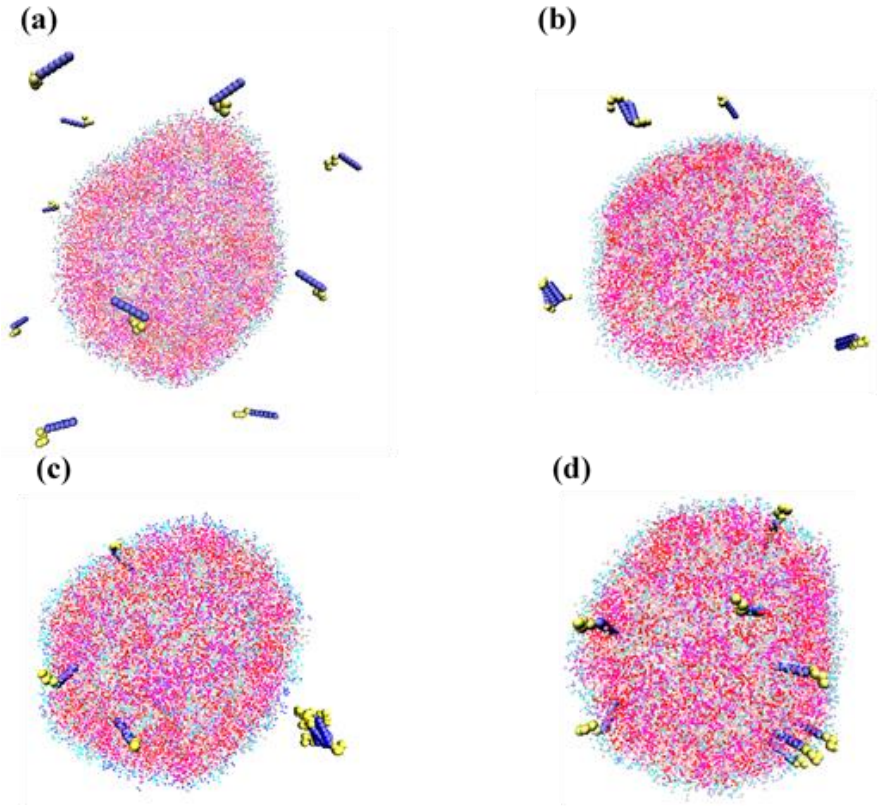

Figure 3.4 System snapshot of system with 10 nanopins and 2301 lipid and cholesterol molecules at time (a) t = 1000 τ, (b) t = 5000 τ, (c) t = 15000 τ, and (d) t = 25000 τ. Not all nanopins are shown for clarity.

The role of the overall hydrophobicity of the nanopins on the insertion dynamics can be understood by repeating the procedure for HN and H1 nanopin architectures. We observe similar trends in the pre-insertion assembly of the nanopins, their capture, rapid insertion into the bilayer and disassembly. These results further corroborate that the nanopin-bilayer association is predominantly driven by interactions between the hydrophobic components.[35,166-169] In earlier studies, nanoparticles and model transmembrane proteins with dimensions much larger than the bilayer amphiphilic molecules, were observed to aggregate in the bilayer.[54-57] This observation is attributed to

depletion-induced attraction. In this study, the disparity in the dimensions of the nanopins and the bilayer amphiphilic molecular species is not significant. The H1 nanopin is 4 r_c in length whereas the bilayer width spans 5 r_c. The conformational entropy of the amphiphilic molecules endows a slightly higher effective dimension than that corresponding to the nanopin. Hence, the presence of the nanopins in the bilayer has minimal impact on the conformational entropy of the neighboring amphiphilic molecules. Therefore, the disassembly of the nanopin aggregate minimizes the free energy by increasing both the translational and orientational entropy of the nanopins

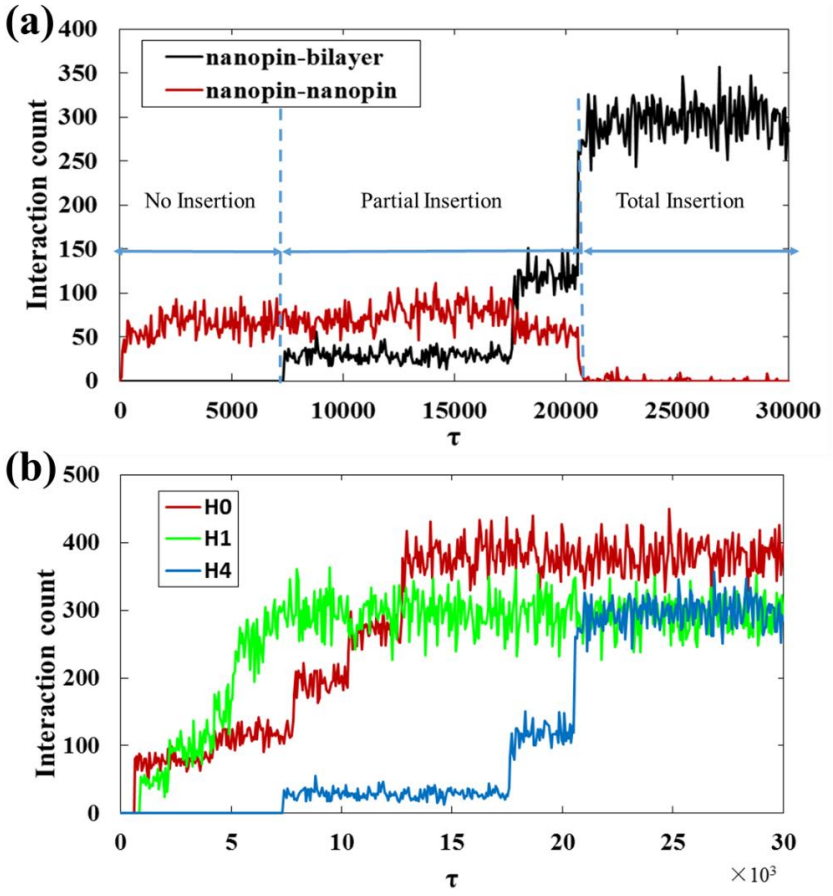

. Figure 3.5 (a) Time evolution of the interaction count between the nanopin H4 and membrane components, and other nanopins, (b) time evolution of the interaction count between bilayer and nanopin H0, H1 and H4 respectively.

We examine the insertion process for ten H4 nanopins (see Fig 3.4) through the time evolution of the interaction count between nanopins, and the nanopins and bilayer components, as shown in Fig 3.5 (a). The aggregation of the nanopins in solution, prior to their insertion into the vesicle bilayer, is captured by the high nanopin-nanopin interaction count. The initial interaction between the nanopins and the membrane is demonstrated by the rise in the nanopin-bilayer interaction count at 7600 τ. The step-wise increase in the nanopin-bilayer interactions indicates the insertion of the aggregates into the bilayer. The nanopin-nanopin interaction becomes negligible when all the inserted aggregates have disassembled into the individual nanopins, as demonstrated by the very low values of the nanopin-nanopin interaction count. The same observations hold for a larger number of inserted nanopins. We report similar trends for nanopin architectures H1 and HN, as shown in Fig. 3.5 (b) but note differences in the nanopin-bilayer interaction counts after all ten nanopins are inserted into the vesicle. We find nanopin architecture HN to have the highest interaction count with components the vesicle bilayer, with negligible difference in the corresponding results for nanopins H1 and H4. The observed difference can be explained by the orientation of the nanopins in the vesicle bilayer, as discussed in the next section.

3.3.3 Distribution of tethers in the monolayers

We observe differences in the orientation of the nanopins inserted in the bilayer as a function of hydrophobicity and architecture, as summarized in Fig. 3.6 Our results show architectures H4 and H1 to adopt orientations that are normal to the bilayer surface with the hydrophilic component exposed to the aqueous region. However, the HN nanopin is observed to adopt a range of orientations including perpendicular to the bilayer normal.

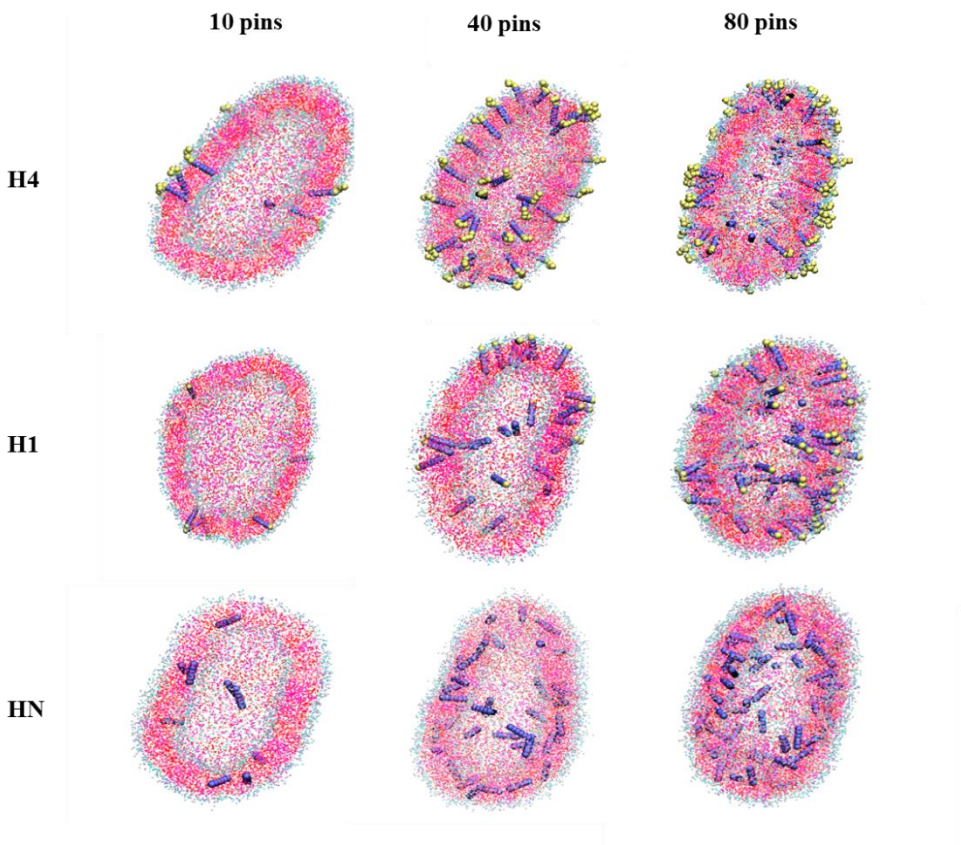

Figure 3.6 Images of ternary vesicle with different number and types of nanopins. Not all nanopins are shown due to the cross-sectional view of the vesicles.

To better understand such discrepancies in the orientations, we examine the angle distributions of the nanopins in the bilayer, as shown in Fig 3.7 We measure the angle between two vectors: the first vector connects the centers of mass of the vesicle and the rigid part of nanopin, and the other vector connects the centers of the two beads located at the extremities of the rigid part of a nanopin. As the vesicle is approximately spherical, the angle measured can be effectively regarded as the tilt angle away from the normal of the local bilayer surface. The angle measurements demonstrate nanopin architectures H1 and H4 to adopt orientations that deviate slightly (35.55^{o} for H1 and 37.22^{o} for H4) from the

bilayer normal. Experimental studies on short amphiphilic transmembrane helices reported a tilting angle of 26° using Solid-State NMR and an angle of 32° using IR dichroism method.[170,171] In comparison, the angle distribution for nanopin architecture HN is observed to be a symmetric Gaussian distribution over the range of 0 to 180 degrees with an average angle of 89.93°. We surmise that the purely hydrophobic architecture favors an orientation that is normal to the bilayer surface to minimize unfavorable interactions with the hydrophilic solvent, and maximize favorable interactions with the hydrocarbon groups in the bilayer. This hypothesis is supported by the large number of interactions of nanopin architecture HN with the hydrophobic components of the vesicle.

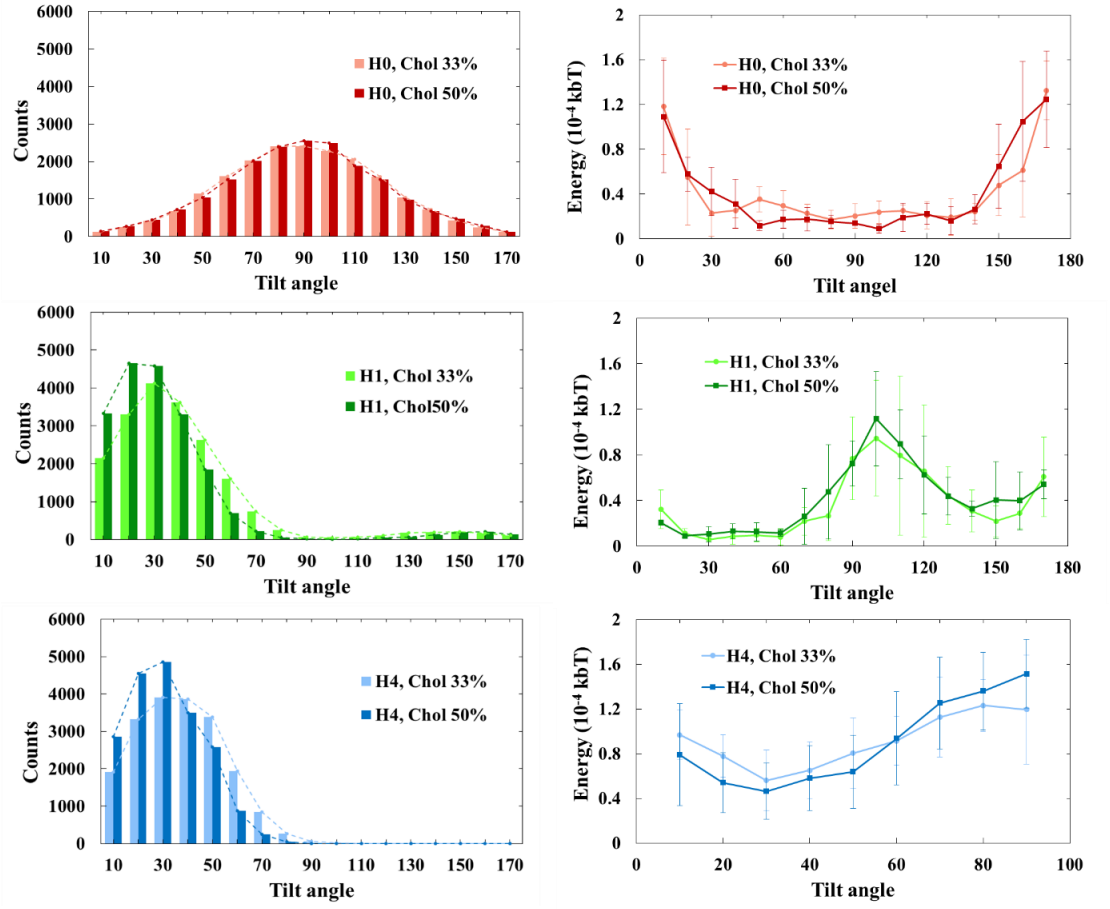

Figure 3.7 Orientation angle and energy distribution for different nanopin architectures and concentrations of cholesterol.

We determine whether the angle distribution for the different types of nanopins is driven by the minimization of the energy of the system. We compute the pair interaction energy of the nanopins with other components of the system for each particular angle that is associated with the angle distribution plot, and draw correspondence with the angle distribution. We observe the trends in the pair interaction energy to complement the angle distribution. Hence, the angle distribution for the three nanopin architectures is driven by minimization of the pair interaction energies. Earlier studies have shown the orientation of transmembrane proteins to be regulated by the hydrophobic mismatch.[117,172-175] For transmembrane proteins with a negative hydrophobic mismatch, the proteins with hydrophilic ends exposed to the aqueous environment have tilt angles close to 0^{o}, while those entirely embedded in the hydrophobic region tend to have random orientations.[175]

3.3.4 Transverse diffusion of nanopins across the monolayers

We find that 5.7 % of the H1 nanopins reside in the inner monolayer of the vesicle such that their hydrophilic head group is exposed to the solvent in the inner cavity of the vesicle. Since all the nanopins are inserted into the outer monolayer of the vesicle from solution, the inverted orientation could result either from the direct penetration of the nanopins into the inner monolayer of the vesicle during the insertion process, or the transverse diffusion of nanopins from the outer to inner monolayer. We observe a spontaneous flip-flop event for a nanopin of architecture H1, as shown in Figure 3.8, to occur after residing in the outer monolayer of the vesicle for a relatively long time interval (~ 15,000 τ).

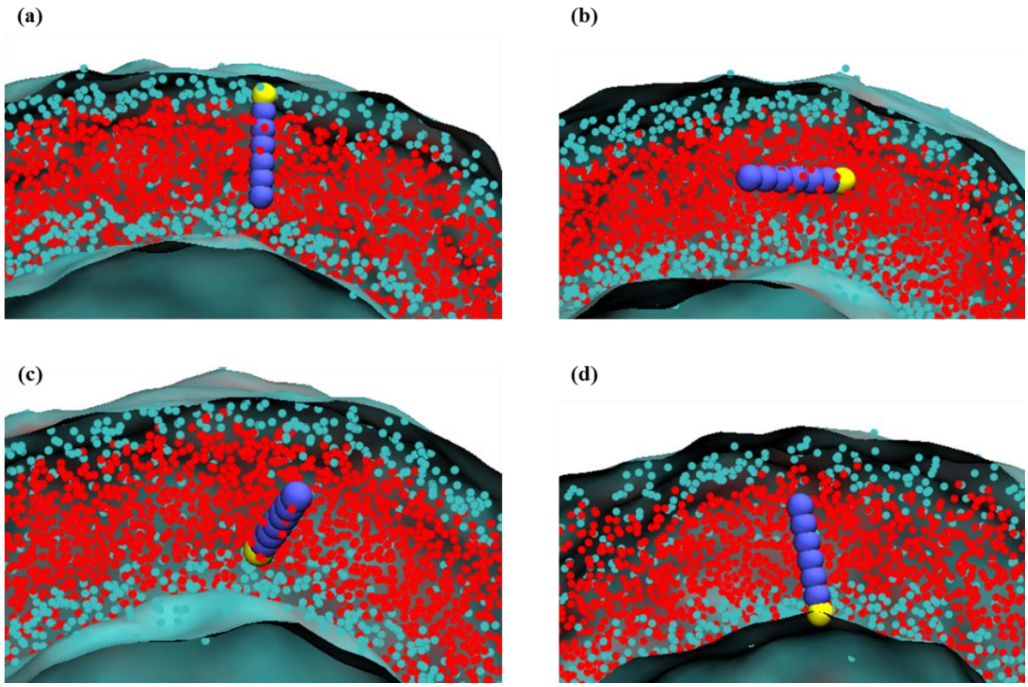

Figure 3.8 Images of a single H1 nanopin undergoing transverse diffusion at time (a) t = 585 τ, (b) t = 625 τ, (c) t = 660 τ, and (d) t = 710 τ.

To understand the occurrence of transverse diffusion for nanopin architecture H1, we note that the orientation of nanopins with hydrophilic moieties are governed by two factors. The first factor is the hydrophobic mismatch between hydrophobic part of the nanopin and the hydrophobic core of the bilayer, and the second factor is the dimension of hydrophilic part of the nanopin. The hydrophobic mismatch tends to drive the nanopins to orientate themselves parallel to local bilayer surface, as shown for nanopin architecture HN which is purely hydrophobic. Since the three nanopin architectures possess identical hydrophobic lengths, we believe that the hydrophobic mismatch effect is the same for all three architectures. For nanopin architecture H4, the unfavorable enthalpic interaction between the hydrophilic hair of the nanopin and the hydrophobic core of the bilayer prohibits the complete immersion of the nanopins into the core of the bilayer. For nanopin architecture H1, the unfavorable enthalpic penalty is not as significant due to the short

length of the hydrophilic part. Hence, nanopin architecture H1 is able to adopt a metastable state which could result in inter-monolayer diffusion or return to its original state. This hypothesis is supported by the time evolution of the interaction count during a transverse diffusion process of a single nanopin H1, as shown in Fig 3.9. The change of orientation (see Fig 3.8 (a), (b)) from parallel to perpendicular (to the bilayer normal) is characterized by the increase in the interaction count between the head group of H1 and the tail groups of the bilayer components, as well as a decrease in the interaction count between the hydrophilic groups of the nanopin and the bilayer components. The perpendicular orientation is maintained for 50 τ before the nanopin assumes an antiparallel orientation to the outward bilayer normal and resumes diffusing in the inner monolayer.

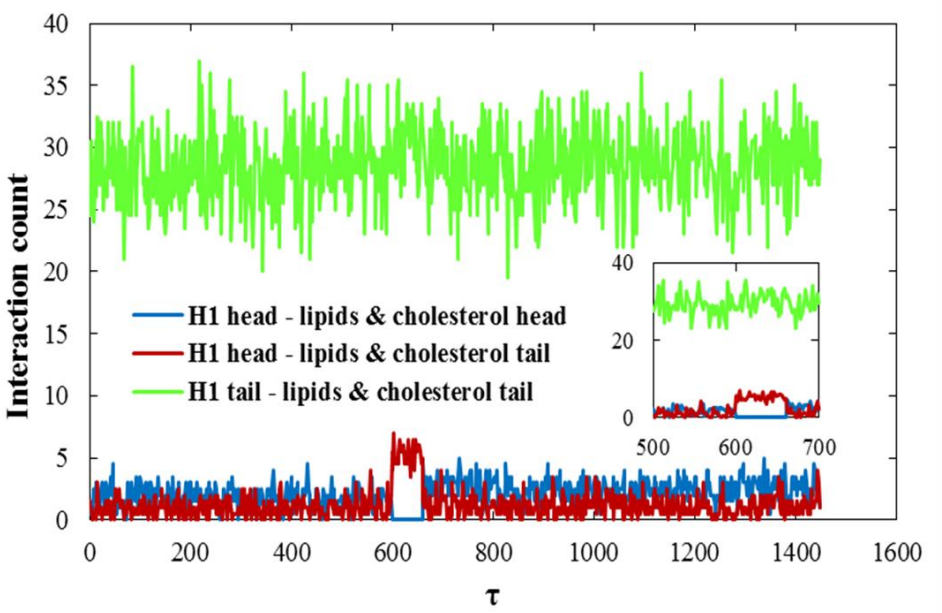

Figure 3.9 Time evolution of the interaction count between different components of the nanopins and the membrane during transverse diffusion of a single H1 nanopin.

We surmise that the transverse diffusion of the nanopins is activated by thermal fluctuations which result in a transient increase in the nanopin-cholesterol interaction count

and an inter-monolayer difference in the number of cholesterol molecules interacting with the nanopin. The fluctuation-induced changes cause the nanopin orientation to deviate from the bilayer normal and adopt a parallel configuration to the bilayer plane, while simultaneously submerging into the hydrophobic region of the bilayer. The enthalpically unfavorable parallel configuration of the nanopin drives it to adopt an orientation that is anti-parallel to the outward bilayer normal. This phenomena of transverse diffusion is also found in both computational and

3.3.5 Role of cholesterol

To understand the role of the concentration of cholesterol on the interaction, capture and insertion of the nanopins into the vesicle bilayer, and their subsequent spatial organization, we repeated the studies using a vesicle with a higher relative concentration of cholesterol (50% cholesterol, 25% DPPC and 25% DMPC). The angle distribution measurements (as shown in Fig 3.7) demonstrate nanopin architectures H1 and H4 to adopt smaller angles with respect to the bilayer normal, in comparison to a bilayer with a lower concentration of cholesterol. In addition, we note that the orientation angle of the nanopins lies within a narrower range. The angle distribution of the HN nanopins does not significantly change with respect to corresponding results for a vesicle with a lower relative concentration of cholesterol. We expect the higher relative concentration of cholesterol in the bilayer to increase its mechanical rigidity, and thereby constrain the nanopins to adopt orientation that are more closely aligned with the bilayer normal. Table 3.1 provides the average orientation angle for each nanopin architecture and bilayers with different relative concentrations of cholesterol.

	H4		H1		H0	
	33% chol	50% chol	33% chol	50% chol	33% chol	50% chol
Average angle (deg)	37.2	30.9	35.5	29.19	89.9	90
Standard deviation (deg)	17.2	14.8	17.1	14.7	31.1	26.7

Table 3.1 Orientation angles for nanopin architecture H4, H1 and H0 in vesicles with 33% and 50% concentration of Cholesterol.

Another consequence of the higher mechanical rigidity of the bilayer is the reduced mobility of the bilayer components and the nanopins. Hence, increasing the bilayer rigidity is also expected to influence the inter-monolayer tranverse diffusion of the nanopins. We observe the translocation count rate for H1 to decrease from 5.7% to 4.2% as the cholesterol mole fraction increases from 33% to 50%. We would like to note that the measurement of the interaction count between the nanopins and the different bilayer components, as shown indicating that there is no preferential interaction of the nanopins with the cholesterol molecules in comparison to the phospholipid molecules.

3.4 Chapter conclusions

In this chapter, via the use of DPD approach, we have examined the interactions of peptide mimetic nanoparticles, or nanopins, with a multi-component vesicle. We investigated the role of the nanopin architecture and cholesterol concentration. The capture of the nanopin by the vesicle bilayer was observed to be activated by the unfavorable enthalpic interactions between the hydrophobic components of the nanopins and the hydrophilic solvent. Some of the nanopins were observed to aggregate in solution prior to the capture by the bilayer, followed by their insertion and disassembly in the bilayer. The architectures of the nanopins were observed to influence their relative orientation within the aggregates prior to capture by the bilayer, and their orientation in the bilayer post-

insertion. Purely hydrophobic nanopins tend to arrange themselves in the hydrophobic region of the bilayer, with their length perpendicular to the surface normal vector of the vesicle. Nanopins with hydrophilic components adopt orientations which expose the hydrophilic groups to the aqueous environment and embeds the hydrophobic components in the hydrophobic region of the vesicle bilayer. Nanopins with a short hydrophilic group are able to overcome the energy barrier to accomplish translocation from the outer leaflet to the inner leaflet of the lipid bilayer. Nanopins with a longer hydrophilic functional group are not observed to participate in transverse diffusion across the monolayers. For higher concentrations of cholesterol in the vesicle bilayer, the nanopins in the bilayer are constrained to adopt a narrow range of angles due to increased rigidity of the bilayer. In addition, we observe the occurrence of transverse diffusion across the bilayer to decrease with cholesterol concentration. Our results can potentially guide the design of nanoscale sensors or probes to interface with living cells for applications in medicine, energy or sustainability.

Chapter 4

Modeling Transportation of Sterically Stable Vesicle in Capillary Flow

4.1 General overview

One of the main challenges faced during transportation through channels is the disruption and rupture of delivery vehicle, resulting in the loss of their cargo[179,180]. The flow-induced shear stresses will reorganize the molecular species on the surface of the vehicle, resulting into change of shape, phase separation and potentially create transient pores.[181-183] Long-lived pores on the surface of the carrier will lead to its rupture and loss of contents. In this chapter, our objective is to investigate the shape characteristics during transport of multicomponent bio-inspired vesicles and sterically stable hybrid carriers through blood vessels that are modeled as cylindrical microfluidic channels.[184,185] We aim to establish the relation between flow characteristics and shape transition, and further correlate them with variation of mechanical properties such as line tension, surface tension and surface stress. With this knowledge, we will be able to determine the critical flow rate at which the vesicle ruptures, and investigate the factors and mechanisms underlying the rupture process. The multi-component vesicles encompass representative amphiphilic molecular species present in biological cell membranes, whereas the sterically stable carriers are composed of end-functionalized amphiphilic molecular species such as PEGylated lipids (PEG= Poly Ethylene Glycol). To achieve our objective, we vary the flow rate, the relative concentration of cholesterol or PEGylated lipids in the vesicle and the PEG length to study their effects on the deformation dynamics and morphology of the

vesicles and carriers. We have adopted a Molecular Dynamics (MD) -based mesoscopic simulation technique entitled Dissipative Particle Dynamics (DPD) (details given in chapter 2) for the investigations presented in this chapter.

4.2 Modeling Methodology

4.2.1 Coarse-graining and parameterization of system components

The individual phospholipid molecules are represented by bead-spring models as shown in Figure 4.1 (a) and (b), and are modeled by a head group comprised of three hydrophilic beads and two hydrocarbon tails represented by three hydrophobic beads each. The hairy lipids, as shown in Figure 4.1 (b), encompass an identical architecture for the phospholipid, with hydrophilic tethers grafted to one of the hydrophilic head beads. The hairs or tethers are modeled by three and six hydrophilic beads. Bond and angle potential functional forms and parameters used for the lipids and tethers in this chapter are similar to those used in chapter 2. Experimental examples of the tethers are polyethylene glycol chains with degrees of polymerization n given by 6 and 12. We select these values of the degree of polymerization to design sterically stabilize hairy vesicles with relatively short polyethylene glycol chains. In addition, earlier theoretical[158] and experimental studies[159,160] show polymers with 6 to 17 EO units to be sufficiently effective for reducing the amount of protein adsorption on a surface at a certain surface coverage.

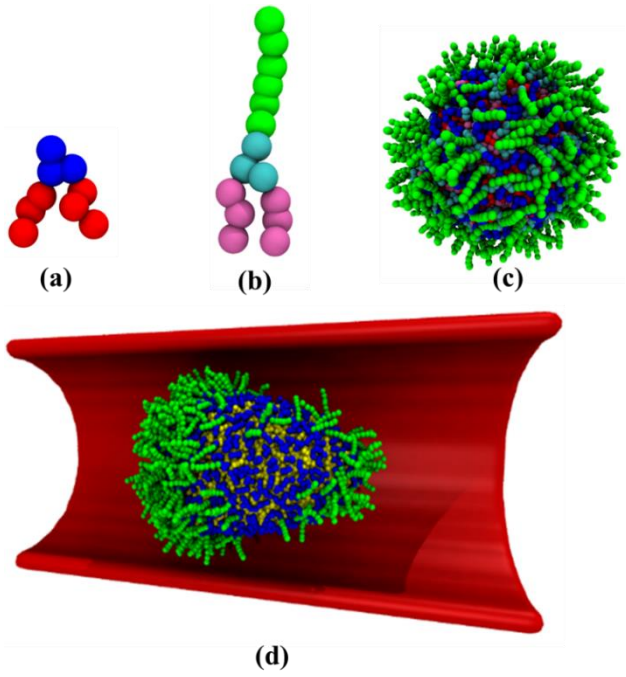

Figure 4.1 Image of coarse-grained model for (a) DPPC, (b) PEGylated DPPC, (c) vesicle with 50% of PEGylated DPPC and 50% of DPPC, (d) vesicle moving in a cylindrical channel, which only have of the channel wall shown and fluid particle is not shown.

The soft repulsive pair potential parameters for the lipid molecule head and tail beads were selected to capture its amphiphilic nature. In addition, the hair beads are considered to be hydrophilic in nature. The soft repulsive interaction parameters between the tethers (T), head (h), and tail (t) beads of lipid types 1 and 2, and the solvent (s) beads are assigned the following values (in units of $k_B T / r_c$): $a_{ss} = 25$, $a_{TT} = 25$, $a_{Ts} = 25$, $a_{h1h1} = 25$, $a_{t1t1} = 25$, $a_{h2h2} = 25$, $a_{t2t2} = 25$, $a_{h1t1} = 100$, $a_{h1s} = 25$, $a_{t1s} = 100$, $a_{h2t2} = 100$, $a_{h2s} = 25$, $a_{t2s} = 100$, $a_{h1T} = 25$, $a_{t1T} = 100$, $a_{h2T} = 25$, $a_{t2T} = 100$, $a_{h1t2} = 100$, $a_{h2t1} = 100$ and $a_{h1h2} = 25$. All the other parameters pertaining to DPD simulation technique, time, length and energy scales are obtained from *chapter 2*.

4.2.2 Fluid building and characterization

In this work, we study the transportation of the hybrid lipid vesicle in a cylindrical channel with Poiseuille flow. The simulations are conducted in an orthogonal box, which has the dimension 40rc*40rc*60rc and is only periodic in the z direction. The channel is a cylindrical space spanning the box with its axis in the z direction. The diameter of the channel is set to be 32 r_c. Wall particles are filled in the rest of the space in the box with bead density $\rho = 3$ and are kept frozen during the simulations. The soft repulsive parameter between wall particles and the other particles is set to be a = 25. To drive the flow, we effectively implement a pressure gradient along the two sides of the channel by adding a constant force on each fluid particle. The flow rate can therefore be tuned by varying the force applied. The repulsion between wall particles and fluid particles serves as a no-slip boundary condition in order to establish Poiseuille flow in the channel. We measure the time average of the velocity of fluid particles with respect to the radial distance, as shown in Figure 4.2 (b). The velocity at fluid-water interface is significantly smaller than (1/10000) the mean velocity of the flow, thus we conclude that our model has achieved a good approximation to Poiseuille flow.

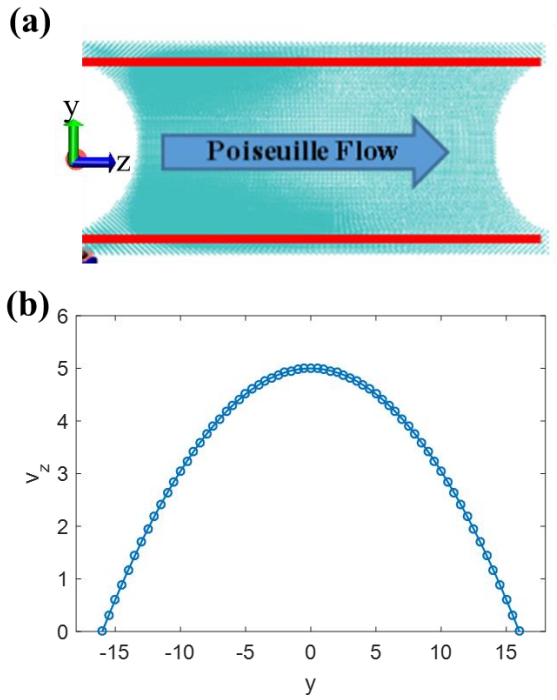

Figure 4.2 (a) Schematic of the systems of modeling Poiseuille flow. (b) The flow velocity profile when a force of $F_0 = 0.005$ is added to all flow particles in the channel

In order to measure the viscosity of the model fluid, we set up an another simulation that only contains fluid particles. We apply a constant force F at z direction for all the particles above the x-y plane and apply -F to the particles below the x-y plane, as suggested in Figure 4.3. The equilibrated velocity profile of the flow indicates a periodic Poiseuille flow which can be partially written as

$$V_x = a\left(Dz - z^2\right) \tag{4.1}$$

A Poiseuille flow in two planar plates has the same form of parabolic velocity profile with

$$a = \frac{\rho g}{2\mu} \tag{4.2}$$

where η is the dynamic viscosity. Here we apply F = 0.05 and we calculate that $a = 0.0509$, therefore $\mu = 1.6028$.

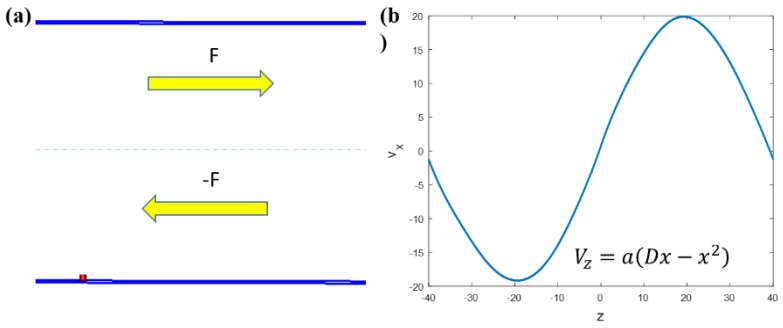

Figure 4.3 (a) Schematic of building periodic Poiseuille flow, (b) flow velocity profile of periodic Poiseuille flow.

Reynolds number Re is then calculated with dynamic viscosity to characterize different flows. We use the following equation,

$$R_e = \frac{\rho U_z D_H}{\mu} \tag{4.3}$$

Where ρ is bead density, we take ρ = 3 globally for both the wall particles and fluid particles. U_z is the mean velocity of the flow and D_H is the diameter of the channel.

4.3 Result and discussion

4.3.1 Shape deformation

We begin with an equilibrated hybrid vesicle in the cylindrical channel with fluid particles surrounded. The simulations are run for $t_0 = 1000\tau$ for pre-equilibration. A timely increasing body force $F = F_0(\frac{t}{t_0} - 1)$ is applied to each fluid particle in the channel in order to avoid rupture of the vesicle by rapid acceleration of the flow. After $t = 2t_0 = 2000\tau$, the force F reaches designated force F_0 and remains constant for the rest 18,000 τ of the simulation. We found that the stable mean flow velocity has a linear relation with F_0 , as shown in Figure 4.4. Therefore, we control the mean flow velocity by varying F_0 ranging from 0 to 0.008.

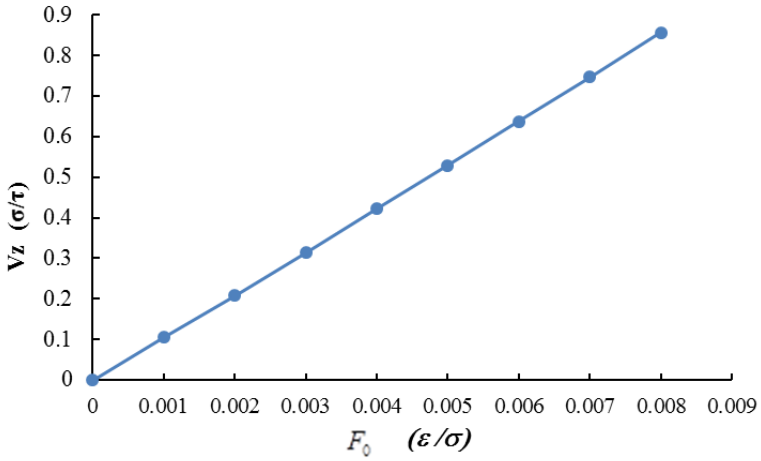

Figure 4.4 Plot of Mean flow velocity as an function of body force that implemented on each flow particle.

When the flow is strong enough we start to observe stable deformation of the shape of the vesicles in flows. Figure 4.5 shows the stable shapes of vesicles with different concentrations of PEGylated lipids and in flows with different Reynolds number. When the flow is slow, and thus the mean flow velocity and Reynolds number are small (U_z < 0.1 r_c / τ, $R_e < 6.3$) , we do not observe significant shape changing of the vesicles for all concentrations of PEGylated lipids tested. These vesicles in motion possess a roughly spherical shape as when no flow is applied. As Reynolds number increases, the shape of the vesicles transit from spherical to bullet like structure with a shaper head in the direction of the flow. We would like to point out that at Re = 40, for vesicle with 10% molar concentration of PEGylated lipids, the shape undergoes a transition from bullet-like to anti-bullet alike or parachute structure which is significantly distinct from vesicles at the same flow condition but with concentration of PEGylated lipids that larger than 20%. Phase separation in the surface is observed for vesicles with large concentrations of tethered lipids and with large Reynolds number, which will be discussed in the next section.

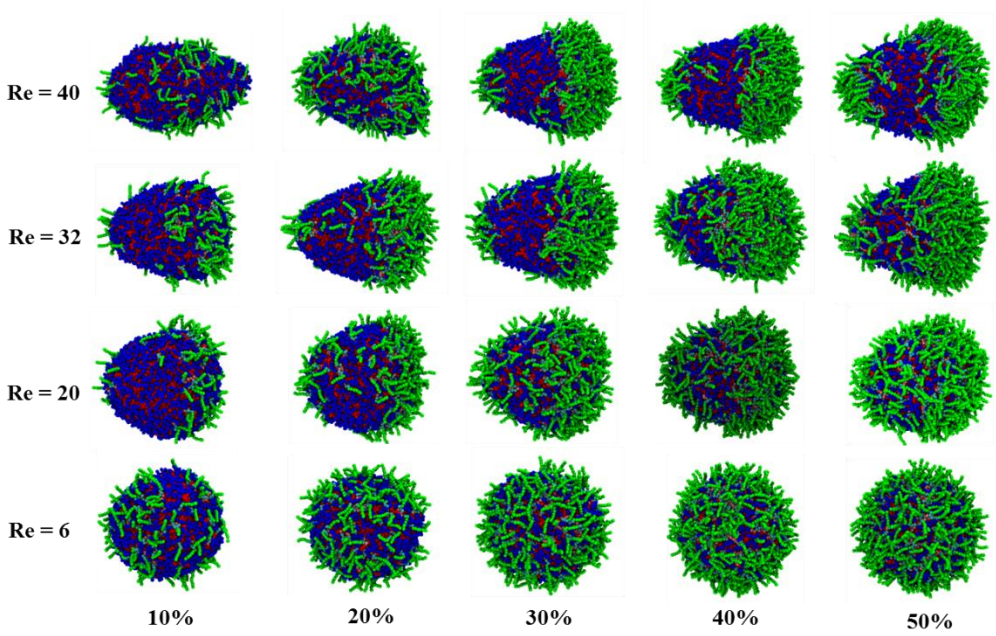

Figure 4.5 Images of equilibrium shapes of vesicles with different concentrations of hairy lipids moving in flows at different Reynolds numbers

To better understand how the deformation of the hybrid vesicle depend on the composition and flow condition, we would like to quantitively measure the shape shaping. The bullet-like shapes are approximately axial symmetric and therefore can be characterized by measuring Deformation Index (DI)[186], which is defined as

$$DI = \frac{X}{Y} - 1$$

where X is the long principle axis and Y is the short principle axis. We measure the DI of vesicles for all concentrations of PEGylatd lipids from 10% to 50% and for Reynolds number with values of 0, 6, 12, 19, 25, 32, 38 and 45, as Figure 4.6 shows. The measurements are performed on equilibrium configurations of the vesicles in flow. We would like to note that we also investigate flow condition with Reynolds number lager than 45 but obtain bicelle as the vesicles ruptures in steady flow during the simulation. Whereas

at Re = 45, vesicles with tethered lipid concentration of 10%, 20% and 30% finally ruptures in steady flow, while vesicles with larger tether concentrations remains their shape integrities and maintain stable bullet-like morphologies. Since DI measurement does not apply into determination of bicelle structures, we do not include these cases in Figure 4.6.

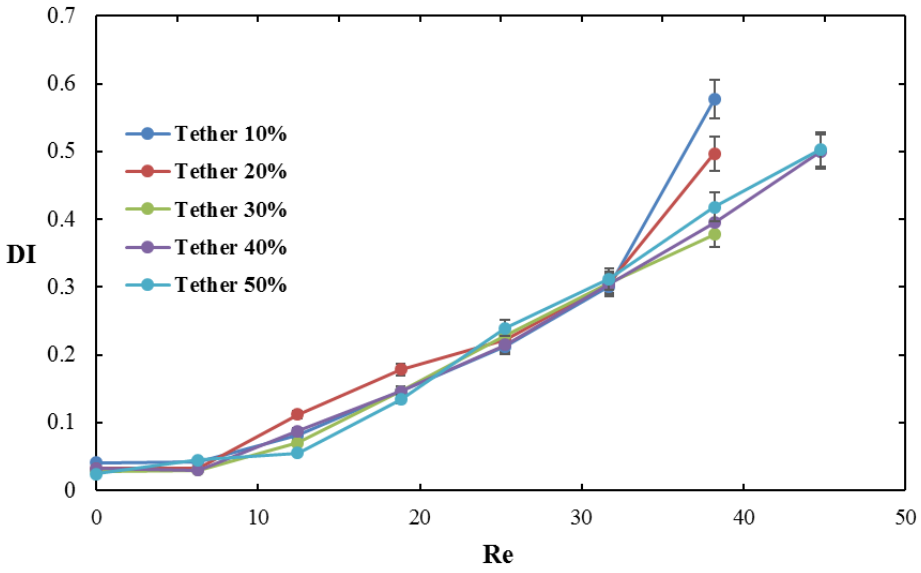

Figure 4.6 Plot of Deformation Index as an function of Reynolds number for vesicles with concentration of hairy lipids of 10%, 20%, 30%, 40% and 50%.

The shape transition from spherical to bullet-like is characterized with a significant linearly increase of the DI when Re is larger than 6, following with another drastic increase of the DI at Re = 32 for tether concentration of 10% and 20% at Re, which indicates another shape transition from bullet-like to parachute-like morphology that lead to earlier rupture. Our results for the DI measurements are in good agreement with our visual observations.

4.3.2 Surface phase separation of hairy vesicle at high Reynolds number

A critical phenomenon that we observe in the deformation of hairy vesicle is that the morphological transition from spherical to bullet-like structure is always coupled with

a significant phase segregation in the surface of the vesicles. We perform further investigation in the interior structure of the vesicle, as shown in Figure 4.7. We found that the binary system is well mixed in the inner monolayer compared to its outer monolayer, indicating that the phase separation only happens in the outer monolayer and it is more likely to be a flow-induced outcome rather than a simultaneous thermodynamic result. It is our hypothesis that the surface phase separation is due to the gradient of local flow velocity of Poiseuille flow with respect to the radial distance to the center axis of the cylindrical channel, as shown in Figure 4.2. The flow particle in the central region move faster than those close to the wall. Such velocity gradient acts a pulling force in the direction of the flow on the head part of the vesicle and a dragging force opposite to direction of the flow on the side part of the vesicle, resulting into a stretch of the shape.

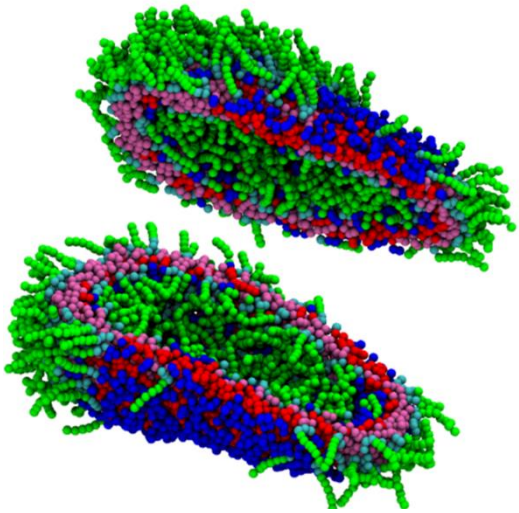

Figure 4.7 Image of a sliced vesicle showing phase separation in the outer monolayer while no phase separation happens in the inner monolayer.

We draw correspondence between the degree of phase segregation and Reynolds number by measuring the interfacial line tension at different flow conditions, as shown in Figure 4.7. The measurements are performed on equilibrium configurations of the binary mixtures, for a range of different concentrations of tethered lipids. The line tension of an

interface separating two phases can be found by calculating the excess free energy per unit length of the contact length along the interface.[176] We estimate the line tension λ of the domain boundary through the following equation[177]

$$\lambda = \left[\frac{1}{2}\left(U_{AA}+U_{BB}\right)-U_{AB}\right]/\mathrm{l}_{\mathrm{mo}} \qquad (4.4)$$

where U_{AA}, $U_{BB,}$ and U_{AB} are the pair interaction energies between components A and B, and l_{mo} is the lateral size of the lipid molecules. The lateral size of the lipid molecules is given by $1.1r_c$ from the area per lipid calculation provided in chapter 2. We would like to note that for Figure 4.8, the last data points of each curve represent the line tension of bicelles from ruptured vesicles at corresponding Reynolds number and hairy lipids concentrations.

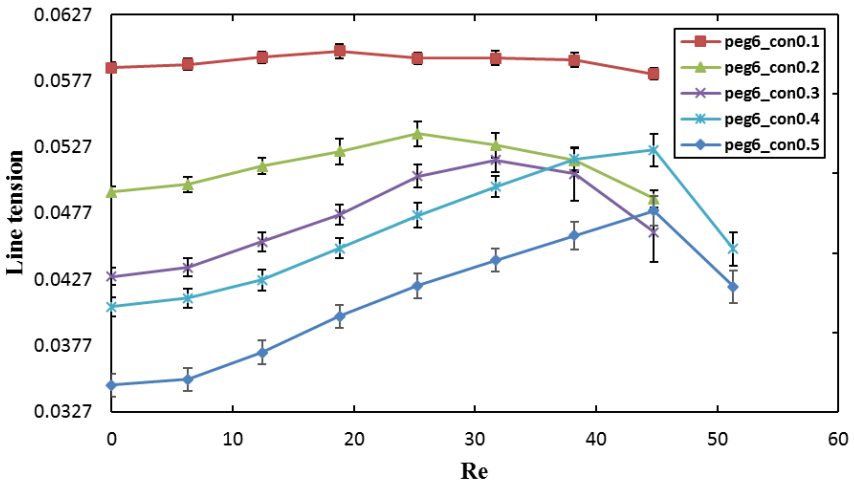

Figure 4.8 Plot of line tension as a function of Reynolds number for vesicles with different concentrations of hairy lipids.

We found that the line tension decreases with increasing concentration of the hairy lipids, which agrees well with previous computational studies.[178] A possible reason to explain this observation is that the increasing excluded volume of the hairs reduces interaction between hairy lipids. For vesicles with hairy lipids concentration higher than

10%, we observe each curve of line tension rapidly increases when Re is larger than 6 and continue to increase until it reaches a maximum, which we call it a stable point. After the stable point, the shape gets unstable because the phase segregation could not be sustained due to a strong perturbation of the flow particles, which is characterized with a drop in the line tension after the stable point and finally reaches rupture point. The relation between line tension and Reynolds number demonstrate that the phase segregation is induced by flow and its level is dependent on the strength of the flow. We also conclude that the stable point approaches the rupture point when a vesicle has more fraction of hairy lipids. It is worthwhile to point out that for hairy lipids concentration of 10% we do not observe a relatively significant variation of line tension at all Reynolds number compared with other concentrations. However, if we plot it solely we would observe that it has a stable point at Re = 20, which is the smallest among all concentrations.

4.4 Chapter conclusions

Via DPD, we developed modeling of Poiseuille flow in cylindrical capillary as well as the transportation of lipid vesicles in the flow. We implement steric stabilization to the lipid vesicle by mixing hairy lipids with phospholipids. We investigated morphological transition of hairy vesicles with different concentration at different flow conditions, which is characterized by Reynolds number. We demonstrate the phase segregation on the surface of hairy vesicles that induced by gradient of flow velocity and can be controlled by varying composition of the vesicle and flow conditions. Our findings can potentially help in the design of drug delivery system with respect to their transport in blood capillaries, and tissue engineering for the design of microfluidic devices with better in-vivo transportation efficiency.

Chapter 5

Conclusions

By utilizing DPD technique, we carried out our investigation on the modeling of interaction between multi-component bio-inspired phospholipid vesicles and peptide-mimetic nanoparticles (nanopins). We demonstrated that hydrophobicity of nanopins and vesicle composition are factors that could affect the behavior of nanopins in terms of aggregation in solution, insertion dynamics, in-bilayer self-organization, self-orientation and transverse diffusion. We extended our investigation into modeling transportation of binary mixture of phospholipid with PEGylated phospholipids and studied the shape variation due to flow conditions and vesicle composition.

In chapter 3, we have examined the interactions of peptide mimetic nanoparticles, or nanopins, with a multi-component vesicle. We investigated the role of the nanopin architecture and cholesterol concentration. The architectures of the nanopins were observed to influence their relative orientation within the aggregates prior to capture by the bilayer, and their orientation in the bilayer post-insertion. Purely hydrophobic nanopins tend to arrange themselves in the hydrophobic region of the bilayer, with their length perpendicular to the surface normal vector of the vesicle. Nanopins with hydrophilic components adopt orientations which expose the hydrophilic groups to the aqueous environment and embeds the hydrophobic components in the hydrophobic region of the vesicle bilayer. Nanopins with a short hydrophilic group are able to overcome the energy barrier to accomplish translocation from the outer leaflet to the inner leaflet of the lipid bilayer. Nanopins with a longer hydrophilic functional group are not observed to participate in transverse diffusion

across the monolayers. For higher concentrations of cholesterol in the vesicle bilayer, the nanopins in the bilayer are constrained to adopt a narrow range of angles due to increased rigidity of the bilayer. In addition, we observe the occurrence of transverse diffusion across the bilayer to decrease with cholesterol concentration. Our results can potentially guide the design of nanoscale sensors or probes to interface with living cells for applications in medicine, energy or sustainability.

In chapter 4, We have examined the transportation of binary vesicles in Poiseuille flow in a cylindrical capillary. The vesicle is composed of tunable concentration of phospholipids and PEGylated phospholipids. We investigated the role of the composition of vesicles and flow conditions on the morphology of the vesicle in flow. We observed shape transitions of the vesicles from spherical to parachute-like shape for low concentration of hairy lipids and from spherical to bullet like shape for high concentrations of hairy lipids. We observed flow-induced surface phase segregation and demonstrated the stabilization effect of hairy lipids by correlating line tension with Reynolds number.

Bibliography

1. Boman, Hans G., Joan Marsh, and Jamie A. Goode. *Antimicrobial peptides*. John Wiley & Sons, 1994.
2. Boman, Hans G. "Antibacterial peptides: key components needed in immunity." *Cell* 65.2 (1991): 205-207.
3. Otvos Jr, Laszlo. "Antibacterial peptides isolated from insects." *Journal of Peptide Science* 6.10 (2000): 497-511.
4. Steiner, Håkan, David Andreu, and Ri B. Merrifield. "Binding and action of cecropin and cecropin analogues: antibacterial peptides from insects."*Biochimica et Biophysica Acta (BBA)-Biomembranes* 939.2 (1988): 260-266.
5. Gudmundsson, Gudmundur H., and Birgitta Agerberth. "Neutrophil antibacterial peptides, multifunctional effector molecules in the mammalian immune system." *Journal of immunological methods* 232.1 (1999): 45-54.
6. Saberwal, Gayatri, and Ramakrishnan Nagaraj. "Cell-lytic and antibacterial peptides that act by perturbing the barrier function of membranes: facets of their conformational features, structure-function correlations and membrane-perturbing abilities." *Biochimica et Biophysica Acta (BBA)-Reviews on Biomembranes* 1197.2 (1994): 109-131.
7. Oren, Ziv, Jiang Hong, and Yechiel Shai. "A repertoire of novel antibacterial diastereomeric peptides with selective cytolytic activity." *Journal of Biological Chemistry* 272.23 (1997): 14643-14649.
8. Zaiou, Mohamed. "Multifunctional antimicrobial peptides: therapeutic targets in several human diseases." *Journal of Molecular Medicine* 85.4 (2007): 317-329.

9. Nordahl, Emma Andersson, et al. "Activation of the complement system generates antibacterial peptides." *Proceedings of the National Academy of Sciences of the United States of America* 101.48 (2004): 16879-16884.
10. Braff, M. H., and R. L. Gallo. "Antimicrobial peptides: an essential component of the skin defensive barrier." *Antimicrobial Peptides and Human Disease*. Springer Berlin Heidelberg, 2006. 91-110.
11. Cudic, Mare, and L. Otvos Jr. "Intracellular targets of antibacterial peptides."*Current drug targets* 3.2 (2002): 101-106.
12. Wieprecht, Torsten, et al. "Influence of the angle subtended by the positively charged helix face on the membrane activity of amphipathic, antibacterial peptides." *Biochemistry* 36.42 (1997): 12869-12880.
13. Rosenfeld, Yosef, and Yechiel Shai. "Lipopolysaccharide (Endotoxin)-host defense antibacterial peptides interactions: role in bacterial resistance and prevention of sepsis." *Biochimica et Biophysica Acta (BBA)-Biomembranes*1758.9 (2006): 1513-1522.
14. Islam, Dilara, et al. "Downregulation of bactericidal peptides in enteric infections: a novel immune escape mechanism with bacterial DNA as a potential regulator." *Nature medicine* 7.2 (2001): 180-185.
15. Otvos, Laszlo. "Antibacterial peptides and proteins with multiple cellular targets." *Journal of Peptide Science* 11.11 (2005): 697-706.
16. Altman, H., et al. "In vitro assessment of antimicrobial peptides as potential agents against several oral bacteria." *Journal of Antimicrobial Chemotherapy*58.1 (2006): 198-201.

17. Lemaitre, Bruno, Jean-Marc Reichhart, and Jules A. Hoffmann. "Drosophila host defense: differential induction of antimicrobial peptide genes after infection by various classes of microorganisms." *Proceedings of the National Academy of Sciences* 94.26 (1997): 14614-14619.
18. Hancock, Robert EW, and Hans-Georg Sahl. "Antimicrobial and host-defense peptides as new anti-infective therapeutic strategies." *Nature biotechnology* 24.12 (2006): 1551-1557.
19. Hoskin, David W., and Ayyalusamy Ramamoorthy. "Studies on anticancer activities of antimicrobial peptides." *Biochimica et Biophysica Acta (BBA)-Biomembranes* 1778.2 (2008): 357-375.
20. Suttmann, Henrik, et al. "Antimicrobial peptides of the Cecropin-family show potent antitumor activity against bladder cancer cells." *BMC urology* 8.1 (2008): 5.
21. Lindgren, Maria, et al. "Cell-penetrating peptides." *Trends in pharmacological sciences* 21.3 (2000): 99-103.
22. Johnson, Randolph M., Stephen D. Harrison, and Derek Maclean. "Therapeutic applications of cell-penetrating peptides." *Cell-Penetrating Peptides*. Humana Press, 2011. 535-551.
23. Zorko, Matjaž, and Ülo Langel. "Cell-penetrating peptides: mechanism and kinetics of cargo delivery." *Advanced drug delivery reviews* 57.4 (2005): 529-545.
24. Gupta, Bhawna, Tatiana S. Levchenko, and Vladimir P. Torchilin. "Intracellular delivery of large molecules and small particles by cell-penetrating proteins and peptides." *Advanced drug delivery reviews* 57.4 (2005): 637-651.
25. Drin, Guillaume, et al. "Studies on the internalization mechanism of cationic cell-

penetrating peptides." *Journal of Biological Chemistry* 278.33 (2003): 31192-31201.

26. Deshayes, S., et al. "Cell-penetrating peptides: tools for intracellular delivery of therapeutics." *Cellular and Molecular Life Sciences CMLS* 62.16 (2005): 1839-1849.
27. Heitz, Frederic, May Catherine Morris, and Gilles Divita. "Twenty years of cell‐penetrating peptides: from molecular mechanisms to therapeutics."*British journal of pharmacology* 157.2 (2009): 195-206.
28. Hällbrink, Mattias, et al. "Cargo delivery kinetics of cell-penetrating peptides." *Biochimica et Biophysica Acta (BBA)-Biomembranes* 1515.2 (2001): 101-109.
29. Mäe, Maarja, and Ülo Langel. "Cell-penetrating peptides as vectors for peptide, protein and oligonucleotide delivery." *Current opinion in pharmacology* 6.5 (2006): 509-514.
30. Duchardt, Falk, et al. "A Comprehensive Model for the Cellular Uptake of Cationic Cell‐penetrating Peptides." *Traffic* 8.7 (2007): 848-866.
31. Pantarotto, Davide, et al. "Translocation of bioactive peptides across cell membranes by carbon nanotubes." *Chemical Communications* 1 (2004): 16-17.
32. Tseng, Yun-Long, Jun-Jen Liu, and Ruey-Long Hong. "Translocation of liposomes into cancer cells by cell-penetrating peptides penetratin and tat: a kinetic and efficacy study." *Molecular pharmacology* 62.4 (2002): 864-872.
33. Patel, Leena N., Jennica L. Zaro, and Wei-Chiang Shen. "Cell penetrating peptides: intracellular pathways and pharmaceutical perspectives."*Pharmaceutical research* 24.11 (2007): 1977-1992.
34. Zhang, Lijuan, Annett Rozek, and Robert EW Hancock. "Interaction of cationic antimicrobial peptides with model membranes." *Journal of Biological*

Chemistry 276.38 (2001): 35714-35722.

35. Matsuzaki, Katsumi, et al. "Translocation of a channel-forming antimicrobial peptide, magainin 2, across lipid bilayers by forming a pore." *Biochemistry*34.19 (1995): 6521-6526.
36. Magzoub, Mazin, and Astrid Gräslund. "Cell-penetrating peptides: small from inception to application." *Quarterly reviews of biophysics* 37.02 (2004): 147-195.
37. Oh, Donghoon, et al. "Antibacterial Activities of Amphiphilic Cyclic Cell-Penetrating Peptides against Multidrug-Resistant Pathogens." *Molecular pharmaceutics* 11.10 (2014): 3528-3536.
38. Westerhoff HV, Juretic D, Hendler RW, Zasloff M. Proc Natl Acad Sci USA 1989;86:6597–601.
39. Lehrer RI, Barton A, Daher KA, Harwig SS, Ganz T, Selsted ME. J Clin Invest 1989;84:553–61.
40. Matsuzaki K, Sugishita K, Harada M, Fujii N, Miyajima K. Biochim Biophys Acta 1997;1327:119–30.
41. da Silva Jr A, Teschke O. Biochim Biophys Acta 2003;1643:95–103.
42. Bechinger B. Biochim Biophys Acta 1999;1462:157–83.
43. Shai Y. Biochim Biophys Acta 1999;1462:55–70.
44. D. Wade, A. Boman, B. Wahlin, C.M. Drain, D. Andreu, H.G. Boman, R.B. Merri¢eld, Proc. Natl. Acad. Sci. USA 87 (1990) 4761-4765
45. R.B. Merri¢eld, E.L. Merri¢eld, P. Juvvadi, D. Andreu, H.G. Boman, Ciba Found. Symp. 186 (1994) 5^20.

46. Geng, Y.; Dalhaimer, P.; Cai, S.; Tsai, R.; Tewari, M.; Minko, T.; Discher, D. E. Shape Effects of Filaments versus Spherical Particles in Flow and Drug Delivery. *Nature Nanotechnology* **2007**, *2*, 249 – 255.

47. Dobereiner, H.-G.; Evans, E.; Kraus, M.; Seifert, U.; Wortis, M. Mapping Vesicle Shapes into the Phase Diagram: A Comparison of Experiment and Theory. *Phys. Rev. E.* **1997**, *55*, 4458.

48. Sandstrom, M. C.; Johansson, E.; Edwards, K. Structure of Mixed Micelles Formed in PEG-Lipid/lipid Dispersions. *Langmuir* **2007**, 23, 4192-4198.

49. Gao, L. H.; Shillcock, J.; Lipowsky, R. Improved Dissipative Particle Dynamics Simulations of Lipid Bilayers. *J. Chem. Phys.* **2007**, 126, 015101.

50. Shillcock, J. C.; Lipowsky, R. EquilibriumSstructure and Lateral Stress Distribution of Amphiphilic Bilayers from Dissipative Particle Dynamics Simulations. *J. Chem. Phys.* **2002**, 117, 5048–5061.

51. Laradji, M.; Kumar, P.B.S. Dynamics of Domain Growth in Self-assembled Fluid Vesicles. *Phys. Rev. Lett.* **2004**, 93, 198105.

52. Kranenburg, M.; Kumar, P.B.S. Dynamics of Domain Growth in Self-assembled Fluid Vesicles. *Phys. Rev. Lett.* **2004**, *93*, 198105.

53. Ramachandran, S.; Laradji, M.; Kumar, P.B.S. Lateral Organization of Lipids in Multi-component Liposomes. *J. Phys. Soc. Jpn.* **2009**, *78*, 041006.

54. Dutt, M.; Kuksenok, O.; Little, S.R.; Balazs, A.C. Designing Tunable Bio-nanostructured Materials via Self-assembly of Amphiphilic Lipids and Functionalized Nanotubes. *MRS Spring 2012 Conference Proceedings* **2012**, 1464.

55. Dutt, M.; Kuksenok, O.; Nayhouse, M. J.; Little, S. R.; Balazs, A. C. Modeling the Self-Assembly of Lipids and Nanotubes in Solution: Forming Vesicles and Bicelles with Transmembrane Nanotube Channels. *ACS Nano* **2011**, *5*, 4769–4782.
56. Dutt, M.; Nayhouse, M.J.; Kuksenok, O.; Little, S.R.; Balazs, A.C. Interactions of End-Functionalized Nanotubes with Lipid Vesicles: Spontaneous Insertion and Nanotube Self-organization. *Current Nanoscience* **2011**, *7*, 699-715.
57. Dutt, M.; Kuksenok, O.; Little, S.R.; Balazs, A.C. Forming Transmembrane Channels Using End-Functionalized Nanotubes. *Nanoscale* **2011**, *3*, 240-250.
58. Ludford, P.; Aydin, F.; Dutt, M. Design and Characterization of Nanostructured Biomaterials via the Self-assembly of Lipids. *MRS Fall 2013 Conference Proceedings* **2013**, 1498.
59. Koufos, E.; Dutt, M. Design of Nanostructured Hybrid Inorganic-biological Materials via Self-assembly. *MRS Spring 2013 Conference Proceedings* **2013**, 1569.
60. Smith, K. A.; Jasnow, D.; Balazs, A. C. Designing Synthetic Vesicles that Engulf Nanoscopic Particles. *J. Chem. Phys.* **2007**, *127*, 084703.
61. Laradji, M.; Kumar, P.B.S. Anomalously Slow Domain Growth in Fluid Membranes with Asymmetric Transbilayer Lipid Distribution. *Phys. Rev. E: Stat., Nonlinear, Soft Matter Phys*. **2006**, *73*, 040910.
62. Illya, G.; Lipowsky, R.; Shillcock, J. C. Two-component Membrane Material Properties and Domain Formation from Dissipative Particle Dynamics. *J. Chem. Phys.* **2006**, *125*, 114710.
63. Groot, R. D.; Warren, P. B. Dissipative Particle Dynamics: Bridging the Gap between Atomistic and Mesoscopic Simulation. *J. Chem. Phys.* **1997**, *107*, 4423–4435.

64. Hoogerbrugge, P. J.; Koelman, J. M. V. A. Simulating Microscopic Hydrodynamic Phenomena with Dissipative Particle Dynamics. *Europhys. Lett.* **1992**, *19*, 155.

65. Alexeev, A.; Upsal W. E.; Balazs, A. C. Harnessing Janus Nanoparticles to Create Controllable Pores in Membranes. *ACS Nano*. **2008**, *2*, 1117–1122.

66. Rekvig, L.; Kranenburg, M.; Vreede, J.; Hafskjold, B.; Smit, B. Investigation of Surfactant Efficiency Using Dissipative Particle Dynamics. *Langmuir*. **2003**, *19*, 8195.

67. Spangler, E. J.; Laradji, M.; Kumar, P.B.S. Anomalous Freezing Behavior of Nanoscale Liposomes. *Soft Matter* **2012**, *8*, 10896-10904.

68. Revalee, J.D.; Laradji, M.; Kumar, P.B.S. Implicit-solvent Mesocale Model based on Soft-core Potentials for Self-assembled Lipid Membranes. *J. Chem. Phys.* **2008**, *128*, 035102.

69. Taniguchi, T. Shape Deformation and Phase Separation Dynamics of Two-component Vesicles. *Phys. Rev. Lett.* **1996**, *76*, 4444-4447.

70. Fan, J.; Han, T.; Haataja, M. Hydrodynamic Effects on Spinodal Decomposition Kinetics in Planar Lipid Bilayer Membranes. *J. Chem. Phys.* **2010**, *133*, 235101.

71. Brown, F. L. H. Continuum Simulations of Biomembrane Dynamics and the Importance of Hydrodynamic Effects. *Q. Rev. Biophys.* **2011**, *44*, 391–432.

72. Yamamoto, Satoru, and Shi-Aki Hyodo. "Budding and fission dynamics of two-component vesicles." The Journal of chemical physics 118.17 (2003): 7937-7943.

73. Laradji, Mohamed, and PB Sunil Kumar. "Domain growth, budding, and fission in phase-separating self-assembled fluid bilayers." *The Journal of chemical physics* 123.22 (2005): 224902.

74. Zheng, Chen, et al. "Phase diagrams for multi-component membrane vesicles: A

coarse-grained modeling study." *Langmuir* 26.15 (2010): 12659-12666.

75. Yamamoto, S.; Maruyama, Y.; Hyodo, S. Dissipative Particle Dynamics Study of Spontaneous Vesicle Formation of Amphiphilic Molecules. J. Chem. Phys. 2002, 116, 5842–5849.
76. Antonietti, M.; Forster, S. Vesicles and Liposomes: A SelfAssembly Principle Beyond Lipids. Adv. Mater. 2003, 15, 1323–1333.
77. Shinoda , W.; De Vane, R.; Klein, M. L. Zwitterionic Lipid Assemblies: Molecular Dynamics Studies of Monolayers, Bilayers and Vesicles Using a New Coarse Grain Force Field. J. Phys. Chem. B 2010, 114, 6836–6849.
78. Noguchi, H.; Takasu, M. Self-Assembly of Amphiphiles into Vesicles: A Brownian Dynamics Simulation. Phys. Rev. E 2001 , 64, 041913.
79. Huang, J.; Wang, Y.; Qian, C. Simulation Study on the Formation of Vesicle and Influence of Solvent. J. Chem. Phys. 2009, 131, 234902.
80. Marrink, S. J.; Mark, A. E. Molecular Dynamics Simulation of the Formation, Structure and Dynamics of Small Phospholipid Vesicles. J. Am. Chem. Soc. 2003, 125, 15233–15242.
81. Marrink, S. J.; Mark, A. E. Simulations of the Spontaneous Aggregation of Phospholipids into Bilayers. J. Am. Chem. Soc. 2003, 125, 15233–15242.
82. Marrink, S. J.; Tieleman, D. P.; Mark, A. E. Molecular Dynamics Simulations of the Kinetics Spontaneous Micelle Formation. J. Am. Chem. Soc. 2003, 125, 15233–15242.
83. Wang, Z.; He, X. Dynamics of Vesicle Formation from Liquid Droplets: Mechanism and Controllability. J. Chem. Phys. 2009, 130, 094905.
84. Fujiwara, S.; Itoh, T.; Hashimoto, M.; Horiuchi, R. Molecular, Dynamics Simulation

of Amphiphilic Molecules in Solution: Micelle Formation and Dynamics Coexistence. J. Chem. Phys. 2009, 130, 144901.

85. Leng, J.; Egelhaaf, S. U.; Cates, M. E. Kinetic Pathway of Spontaneous Vesicle Formation. Europhys. Lett. 2002, 59, 311 –317.
86. Leng, J.; Egelhaaf, S. U.; Cates, M. E. Kinetics of Micelle-toVesicle Transition: Aqueous Lecithin-Bile Salt Mixtures. Biophys. J. 2003, 85, 1624–1646.
87. Noguchi, H.; Gompper, G. Dynamics of Vesicle Self-Assembly and Dissolution. J. Chem. Phys. 2006, 125, 164908.
88. Goetz, R.; Gompper, G.; Lipowsky, R. Mobility and Elasticity of Self-Assembled Membranes. Phys. Rev. Lett. 1999, 82, 221 –224.
89. Goetz, R.; Lipowsky, R. Computer Simulations of Bilayer Membranes: Self-Assembly and Interfacial Tension. J. Chem. Phys. 1998, 108, 7397–7409.
90. Cooke, I. R.; Deserno, M. Solvent-free Model for SelfAssembling Fluid Bilayer Membranes: Stabilization of the Fluid Phase Based on Broad Attractive Tail Potentials. J. Chem. Phys. 2005, 123, 224710.
91. Cooke, I. R.; Deserno, M. Coupling Between Lipid Shape and Membrane Curvature. Biophys. J. 2006, 91, 487–495.
92. Wang, Z.-J.; Deserno, M. A Systematically Coarse-Grained Solvent-free Model for Quantitative Phospholipid Bilayer Simulations. J. Phys. Chem. B 2010, 114, 11207–11220.
93. Weiss, T. M.; Narayanan, T.; Wolf, C.; Gradzielski, M.; Panine, P.; Finet, S.; Helsby, W. I. Dynamics of the Self-Assembly of Unilamellar Vesicles. Phys. Rev. Lett. 2005, 94, 038303.

94. Weiss, T. M.; Narayanan, T.; Gradzielski, M. Dynamics of Spontaneous Vesicle Formation in Fluorocarbon and Hydrocarbon Surfactant Mixtures. Langmuir 2008, 24, 3759–3766.

95. Shioi, A.; Hatton, T. A. Model for Formation and Growth of Vesicles in Mixed Anionic/Cationic (SOS/CTAB) Surfactant Systems. Langmuir 2002, 18, 7341 –7348.

96. Allen, M.P.; Tildesley, D.J. Computer Simulations of Liquids. *Clarendon Press*, Oxford, 2001.

97. Nagle, J. F.; Tristram-Nagle, S. Structure of Lipid Bilayers. *Biochim. Biophys. Acta* **2000**, *1469*, 159.

98. Frenkel, D.; Smit, B. Understanding Molecular Simulations: From Algorithms to Applications. *Academic Press*, San Diego, 2002.

99. Rosso, J.; Zachowski, A.; Devaux, P. F., Influence of Chlorpromazine on the Transverse Mobility of Phospholipids in the Human-Erythrocyte Membrane-Relation to Shape Changes. *Biochimica Et Biophysica Acta* **1988,** *942* (2), 271-279.

100. Schrier, S. L.; Zachowski, A.; Devaux, P. F., Mechanisms of Amphipath-Induced Stomatocytosis in Human Erythrocytes. *Blood* **1992,** *79* (3), 782-786.

101. Shai, Y., Mechanism of the Binding, Insertion and Destabilization of Phospholipid Bilayer Membranes by Alpha-Helical Antimicrobial and Cell Non-Selective Membrane-Lytic Peptides. *Biochimica Et Biophysica Acta-Biomembranes* **1999,** *1462* (1-2), 55-70.

102. Oren, Z.; Shai, Y., Mode of Action of Linear Amphipathic Alpha-Helical Antimicrobial Peptides. *Biopolymers* **1998,** *47* (6), 451-463.

103. Bechinger, B., The Structure, Dynamics and Orientation of Antimicrobial Peptides in

Membranes by Multidimensional Solid-State NMR Spectroscopy. *Biochimica Et Biophysica Acta-Biomembranes* **1999,** *1462* (1-2), 157-183.

104. Sakai, N.; Mareda, J.; Matile, S., Rigid-Rod Molecules in Biomembrane Models: From Hydrogen-Bonded Chains to Synthetic Multifunctional Pores. *Accounts of Chemical Research* **2005,** *38* (2), 79-87.

105. Cornelissen, J.; Fischer, M.; Sommerdijk, N.; Nolte, R. J. M., Helical Superstructures from Charged Poly(styrene)-Poly(isocyanodipeptide) Block Copolymers. *Science* **1998,** *280* (5368), 1427-1430.

106. Bhosale, S.; Sisson, A. L.; Sakai, N.; Matile, S., Synthetic Functional π-Stack Architecture in Lipid Bilayers. *Organic & Biomolecular Chemistry* **2006,** *4* (16), 3031-3039.

107. Findlay, B.; Zhanel, G. G.; Schweizer, F., Cationic Amphiphiles, a New Generation of Antimicrobials Inspired by the Natural Antimicrobial Peptide Scaffold. *Antimicrobial Agents and Chemotherapy* **2010,** *54* (10), 4049-4058.

108. Ishitsuka, Y.; Arnt, L.; Majewski, J.; Frey, S. L.; Ratajczak, M.; Kjaer, K.; Tew, G. N.; Lee, K. Y. C., Amphiphilic Poly(phenyleneethynylene)s Can Mimic Antimicrobial Peptide Membrane Disordering Effect by Membrane Insertion (vol 128, pg 13123, 2006). *Journal of the American Chemical Society* **2008,** *130* (7), 2372-2372.

109. Tew, G. N.; Liu, D. H.; Chen, B.; Doerksen, R. J.; Kaplan, J.; Carroll, P. J.; Klein, M. L.; DeGrado, W. F., De novo Design of Biomimetic Antimicrobial Polymers. *Proceedings of the National Academy of Sciences of the United States of America* **2002,** *99* (8), 5110-5114.

110. Gabriel, G. J.; Madkour, A. E.; Dabkowski, J. M.; Nelson, C. F.; Nusslein, K.; Tew,

G. N., Synthetic Mimic of Antimicrobial Peptide with Nonmembrane-Disrupting Antibacterial Properties. *Biomacromolecules* **2008,** *9* (11), 2980-2983.

111. Tang, H.; Doerksen, R. J.; Jones, T. V.; Klein, M. L.; Tew, G. N., Biomimetic Facially Amphiphilic Antibacterial Oligomers with Conformationally Stiff Backbones. Chemistry & Biology 2006, 13 (4), 427-435.

112. Oh, N. M.; Oh, K. T.; Youn, Y. S.; Lee, E. S., Artificial Nano-Pin as a Temporal Molecular Glue for the Targeting of Acidic Tumor cells. *Polymers for Advanced Technologies* **2014,** *25* (8), 842-850.

113. Radzishevsky, I. S.; Rotem, S.; Bourdetsky, D.; Navon-Venezia, S.; Carmeli, Y.; Mor, A., Improved Antimicrobial Peptides Based on Acyl-Lysine Oligomers. *Nature Biotechnology* **2007,** *25* (6), 657-659.

114. Graham, D. Y.; Shiotani, A., New Concepts of Resistance in the Treatment of Helicobacter Pylori Infections. *Nature Clinical Practice Gastroenterology & Hepatology* **2008,** *5* (6), 321-331.

115. Leszczynska, K.; Namiot, A.; Fein, D. E.; Wen, Q.; Namiot, Z.; Savage, P. B.; Diamond, S.; Janmey, P. A.; Bucki, R., Bactericidal Activities of the Cationic Steroid CSA-13 and the Cathelicidin Peptide LL-37 against Helicobacter Pylori in Simulated Gastric Juice. *Bmc Microbiology* **2009,** *9*.

116. Benjamini, A.; Smit, B., Robust Driving Forces for Transmembrane Helix Packing. *Biophysical Journal* **2012,** *103* (6), 1227-1235.

117. Ren, J. H.; Lew, S.; Wang, J. Y.; London, E., Control of the Transmembrane Orientation and Interhelical Interactions within Membranes by Hydrophobic Helix Length. *Biochemistry* **1999,** *38* (18), 5905-5912.

118. Farago, O., "Water-Free" Computer Model for Fluid Bilayer Membranes. *Journal of Chemical Physics* **2003,** *119* (1), 596-605.

119. Brannigan, G.; Brown, F. L. H., Solvent-Free Simulations of Fluid Membrane Bilayers. *Journal of Chemical Physics* **2004,** *120* (2), 1059-1071.

120. Shillcock, J. C., Spontaneous Vesicle Self-Assembly: A Mesoscopic View of Membrane Dynamics. *Langmuir* **2012,** *28* (1), 541-547.

121. Tieleman, D. P.; Leontiadou, H.; Mark, A. E.; Marrink, S. J., Simulation of Pore Formation in Lipid Bilayers by Mechanical Stress and Electric Fields. *Journal of the American Chemical Society* **2003,** *125* (21), 6382-6383.

122. Damodaran, K. V.; Merz, K. M., A Comparison of DMPC-Based and DLPE-Based Lipid Bilayers. *Biophysical Journal* **1994,** *66* (4), 1076-1087.

123. Moore, P. B.; Lopez, C. F.; Klein, M. L., Dynamical Properties of a Hydrated Lipid Bilayer from a Multinanosecond Molecular Dynamics Simulation. *Biophysical Journal* **2001,** *81* (5), 2484-2494.

124. Essmann, U.; Perera, L.; Berkowitz, M. L., The Origin of the Hydration Interaction of Lipid Bilayers from MD Simulation of Dipalmitoylphosphatidylcholine Membranes in Gel and Liquid-Crystalline Phases. *Langmuir* **1995,** *11* (11), 4519-4531.

125. Cooke, I. R.; Deserno, M., Solvent-Free Model for Self-Assembling Fluid Bilayer Membranes: Stabilization of the Fluid Phase Based on Broad Attractive Tail Potentials. *Journal of Chemical Physics* **2005,** *123* (22).

126. West, B.; Schmid, F., Fluctuations and Elastic Properties of Lipid Membranes in the Gel L-Beta ' State: a Coarse-Grained Monte Carlo Study. *Soft Matter* **2010,** *6* (6), 1275-1280.

127. Farago, O., Mode Excitation Monte Carlo Simulations of Mesoscopically Large Membranes. *Journal of Chemical Physics* **2008,** *128* (18).

128. Farago, O., Fluctuation-Induced Attraction between Adhesion Sites of Supported Membranes. *Physical Review E* **2010,** *81* (5).

129. Stevens, M. J.; Hoh, J. H.; Woolf, T. B., Insights into the Molecular Mechanism of Membrane Fusion from Simulation: Evidence for the Association of Splayed Tails. *Physical Review Letters* **2003,** *91* (18).

130. Marrink, S. J.; Risselada, H. J.; Yefimov, S.; Tieleman, D. P.; de Vries, A. H., The MARTINI Force Field: Coarse Grained Model for Biomolecular Simulations. *Journal of Physical Chemistry B* **2007,** *111* (27), 7812-7824.

131. Noguchi, H., Fusion and Toroidal Formation of Vesicles by Mechanical Forces: A Brownian Dynamics Simulation. *Journal of Chemical Physics* **2002,** *117* (17), 8130-8137.

132. Katsov, K.; Muller, M.; Schick, M., Field Theoretic Study of Bilayer Membrane Fusion. I. Hemifusion Mechanism. *Biophysical Journal* **2004,** *87* (5), 3277-3290.

133. May, S.; Kozlovsky, Y.; Ben-Shaul, A.; Kozlov, M. M., Tilt Modulus of a Lipid Monolayer. *European Physical Journal E* **2004,** *14* (3), 299-308.

134. Lee, W. B.; Mezzenga, R.; Fredrickson, G. H., Self-Consistent Field Theory for Lipid-Based Liquid Crystals: Hydrogen Bonding Effect. *Journal of Chemical Physics* **2008,** *128* (7).

135. Ginzburg, V. V.; Balijepailli, S., Modeling the Thermodynamics of the Interaction of Nanoparticles with Cell Membranes. *Nano Letters* **2007,** *7* (12), 3716-3722.

136. Ayton, G.; Voth, G. A., Bridging Microscopic and Mesoscopic Simulations of Lipid

Bilayers. *Biophysical Journal* **2002,** *83* (6), 3357-3370.

137. Wang, Z. J.; Deserno, M., A Systematically Coarse-Grained Solvent-Free Model for Quantitative Phospholipid Bilayer Simulations. *Journal of Physical Chemistry B* **2010,** *114* (34), 11207-11220.

138. Ge, Z. P.; Li, Q.; Wang, Y., Free Energy Calculation of Nanodiamond-Membrane Association-The Effect of Shape and Surface Functionalization. *Journal of Chemical Theory and Computation* **2014,** *10* (7), 2751-2758.

139. Van Lehn, R. C.; Ricci, M.; Silva, P. H. J.; Andreozzi, P.; Reguera, J.; Voitchovsky, K.; Stellacci, F.; Alexander-Katz, A., Lipid Tail Protrusions Mediate the Insertion of Nanoparticles into Model Cell Membranes. *Nature Communications* **2014,** *5*.

140. Wong-Ekkabut, J.; Baoukina, S.; Triampo, W.; Tang, I. M.; Tieleman, D. P.; Monticelli, L., Computer Simulation Study of Fullerene Translocation through Lipid Membranes. *Nature Nanotechnology* **2008,** *3* (6), 363-368.

141. Li, Y.; Chen, X.; Gu, N., Computational Investigation of Interaction between Nanoparticles and Membranes: Hydrophobic/Hydrophilic Effect. *Journal of Physical Chemistry B* **2008,** *112* (51), 16647-16653.

142. Huang, C. J.; Zhang, Y.; Yuan, H. Y.; Gao, H. J.; Zhang, S. L., Role of Nanoparticle Geometry in Endocytosis: Laying Down to Stand Up. *Nano Letters* **2013,** *13* (9), 4546-4550.

143. Shi, X. H.; von dem Bussche, A.; Hurt, R. H.; Kane, A. B.; Gao, H. J., Cell Entry of One-Dimensional Nanomaterials Occurs by Tip Recognition and Rotation. *Nature Nanotechnology* **2011,** *6* (11), 714-719.

144. Kranenburg, M.; Venturoli, M.; Smit, B., Phase Behavior and Induced Interdigitation

in Bilayers Studied with Dissipative Particle Dynamics. *Journal of Physical Chemistry B* **2003,** *107* (41), 11491-11501.

145. Chou, S. H.; Tsao, H. K.; Sheng, Y. J., Morphologies of Multicompartment Micelles Formed by Triblock Copolymers. *Journal of Chemical Physics* **2006,** *125* (19).

146. Ortiz, V.; Nielsen, S. O.; Discher, D. E.; Klein, M. L.; Lipowsky, R.; Shillcock, J., Dissipative Particle Dynamics Simulations of Polymersomes. *Journal of Physical Chemistry B* **2005,** *109* (37), 17708-17714.

147. Boek, E. S.; Coveney, P. V.; Lekkerkerker, H. N. W.; vanderSchoot, P., Simulating the Rheology of Dense Colloidal Suspensions Using Dissipative Particle Dynamics. *Physical Review E* **1997,** *55* (3), 3124-3133.

148. Spenley, N. A., Scaling Laws for Polymers in Dissipative Particle Dynamics. *Europhysics Letters* **2000,** *49* (4), 534-540.

149. Fan, X. J.; Phan-Thien, N.; Chen, S.; Wu, X. H.; Ng, T. Y., Simulating Flow of DNA Suspension Using Dissipative Particle Dynamics. *Physics of Fluids* **2006,** *18* (6).

150. Chen, S.; Phan-Thien, N.; Fan, X. J.; Khoo, B. C., Dissipative Particle Dynamics Simulation of Polymer Drops in a Periodic Shear Flow. *Journal of Non-Newtonian Fluid Mechanics* **2004,** *118* (1), 65-81.

151. Arai, N.; Yasuoka, K.; Zeng, X. C., A Vesicle Cell under Collision with a Janus or Homogeneous Nanoparticle: Translocation Dynamics and Late-Stage Morphology. *Nanoscale* **2013,** *5* (19), 9089-9100.

152. Yang, K.; Ma, Y. Q., Computer Simulation of the Translocation of Nanoparticles with Different Shapes across a Lipid Bilayer. *Nature Nanotechnology* **2010,** *5* (8), 579-583.

153. Ding, H. M.; Tian, W. D.; Ma, Y. Q., Designing Nanoparticle Translocation through

Membranes by Computer Simulations. *Acs Nano* **2012,** *6* (2), 1230-1238.

154. Chen, X. M.; Tian, F. L.; Zhang, X. R.; Wang, W. C., Internalization Pathways of Nanoparticles and Their Interaction with a Vesicle. Soft Matter 2013, 9 (31), 7592-7600.

155. Lins, L.; Charloteaux, B.; Thomas, A.; Brasseur, R., Computational Study of Lipid-Destabilizing Protein Fragments: Towards a Comprehensive View of Tilted Peptides. *Proteins-Structure Function and Genetics* **2001,** *44* (4), 435-447.

156. El Kirat, K.; Lins, L.; Brasseur, R.; Dufrene, Y. F., Fusogenic Tilted Peptides Induce Nanoscale Holes in Supported Phosphatidylcholine Bilayers. *Langmuir* **2005,** *21* (7), 3116-3121.

157. Colherinhas, G.; Fileti, E., Molecular Dynamics Study of Surfactant-Like Peptide Based Nanostructures. *Journal of Physical Chemistry B* **2014,** *118* (42), 12215-12222.

158. Walther, F. J.; Waring, A. J.; Hernandez-Juviel, J. M.; Ruchala, P.; Wang, Z. D.; Notter, R. H.; Gordon, L. M., Surfactant Protein C Peptides with Salt-Bridges ("ion-locks") Promote High Surfactant Activities by Mimicking the Alpha-Helix and Membrane Topography of the Native Protein. *Peerj* **2014,** *2*.

159. Schreier, S.; Malheiros, S. V. P.; de Paula, E., Surface Active Drugs: Self-Association and Interaction with Membranes and Surfactants. Physicochemical and Biological Aspects. *Biochimica Et Biophysica Acta-Biomembranes* **2000,** *1508* (1-2), 210-234.

160. Aydin, F.; Ludford, P.; Dutt, M., Phase Segregation in Bio-Inspired Multi-Component Vesicles Encompassing Double Tail Phospholipid Species. *Soft Matter* **2014,** *10* (32), 6096-6108.

161. Binder, H.; Lindblom, G., Charge-Dependent Translocation of the Trojan Peptide

Penetratin across Lipid Membranes. *Biophysical Journal* **2003,** *85* (2), 982-995.

162. Oren, Z.; Shai, Y., Cyclization of a Cytolytic Amphipathic Alpha-Helical Peptide and Its Diastereomer: Effect on Structure, Interaction with Model Membranes, and Biological Function. *Biochemistry* **2000,** *39* (20), 6103-6114.

163. Kustanovich, I.; Shalev, D. E.; Mikhlin, M.; Gaidukov, L.; Mor, A., Structural Requirements for Potent versus Selective Cytotoxicity for Antimicrobial Dermaseptin S4 Derivatives. *Journal of Biological Chemistry* **2002,** *277* (19), 16941-16951.

164. Stella, L.; Mazzuca, C.; Venanzi, M.; Palleschi, A.; Didone, M.; Formaggio, F.; Toniolo, C.; Pispisa, B., Aggregation and Water-Membrane Partition as Major Determinants of the Activity of the Antibiotic Peptide Trichogin GA IV. *Biophysical Journal* **2004,** *86* (2), 936-945.

165. Radzishevsky, I. S.; Rotem, S.; Zaknoon, F.; Gaidukov, L.; Dagan, A.; Mor, A., Effects of Acyl versus Aminoacyl Conjugation on the Properties of Antimicrobial Peptides. *Antimicrobial Agents and Chemotherapy* **2005,** *49* (6), 2412-2420.

166. Blondelle, S. E.; Houghten, R. A., Design of Model Amphipathic Peptides Having Potent Antimicrobial Activities. *Biochemistry* **1992,** *31* (50), 12688-12694.

167. Wieprecht, T.; Dathe, M.; Epand, R. M.; Beyermann, M.; Krause, E.; Maloy, W. L.; MacDonald, D. L.; Bienert, M., Influence of the Angle Subtended by the Positively Charged Helix Face on the Membrane Activity of Amphipathic, Antibacterial Peptides. *Biochemistry* **1997,** *36* (42), 12869-12880.

168. Wieprecht, T.; Dathe, M.; Krause, E.; Beyermann, M.; Maloy, W. L.; MacDonald, D. L.; Bienert, M., Modulation of Membrane Activity of Amphipathic, Antibacterial Peptides by Slight Modifications of the Hydrophobic Moment. *Febs Letters* **1997,** *417*

(1), 135-140.

169. Tytler, E. M.; Segrest, J. P.; Epand, R. M.; Nie, S. Q.; Epand, R. F.; Mishra, V. K.; Venkatachalapathi, Y. V.; Anantharamaiah, G. M., Reciprocal Effects of Apolipoprotein and Analogs on Membranes-Cross-Sectional Molecular Shapes of Amphipathic-Alpha Helixes Control Membrane Stability. *Journal of Biological Chemistry* **1993,** *268* (29), 22112-22118.

170. Marassi, F. M.; Opella, S. J., Simultaneous Assignment and Structure Determination of a Membrane Protein from NMR Orientational Restraints. *Protein Science* **2003,** *12* (3), 403-411.

171. Kukol, A.; Arkin, I. T., Vpu Transmembrane Peptide Structure Obtained by Site-Specific Fourier Transform Infrared Dichroism and Global Molecular Dynamics Searching. *Biophysical Journal* **1999,** *77* (3), 1594-1601.

172. Park, S. H.; Opella, S. J., Tilt Angle of a Trans-Membrane Helix is Determined by Hydrophobic Mismatch. *Journal of Molecular Biology* **2005,** *350* (2), 310-318.

173. Killian, J. A., Hydrophobic Mismatch between Proteins and Lipids in Membranes. *Biochimica Et Biophysica Acta-Reviews on Biomembranes* **1998,** *1376* (3), 401-416.

174. Bond, P. J.; Sansom, M. S. P., Insertion and Assembly of Membrane Proteins via Simulation. *Journal of the American Chemical Society* **2006,** *128* (8), 2697-2704.

175. Kandasamy, S. K.; Larson, R. G., Molecular Dynamics Simulations of Model Trans-Membrane Peptides in Lipid Bilayers: A Systematic Investigation of Hydrophobic Mismatch. *Biophysical Journal* **2006,** *90* (7), 2326-2343.

176. Weijs, J. H.; Marchand, A.; Andreotti, B.; Lohse, D.; Snoeijer, J. H. Origin of Line Tension for a Lennard-Jones Nanodroplet. *Phys. Fluids* **2011**, *23*, 022001.

177. Lipowsky, R.; Dimova, R. Domains in Membranes and Vesicles. *J. Phys.: Condens. Matter*, **2003**, *15*, 31–45.

178. Shinoda, W.; Discher, D. E.; Klein, M. L.; Loverde, S. M. Probing the Structure of PEGylated-Lipid Assemblies by Coarsegrained Molecular Dynamics. *Soft Matter* 2013, 9, 11549−11556.

179. Zhao, Q.; Han, B.; Wang, Z.; et al. Hollow chitosan-alginate multilayer microcapsules as drug delivery vehicle: doxorubicin loading and in vitro and in vivo studies. *Nanomedicine: Nanotechnology, Biology and Medicine* 2007, *3.1*, 63-74.

180. Johnsen, K. B.; Gudbergsson, J. M.; Skov, M. N.; Pilgaard, L.; Moos, T.; Duroux, M. A. Comprehensive overview of exosomes as drug delivery vehicles—endogenous nanocarriers for targeted cancer therapy. *Biochimica et Biophysica Acta (BBA)-Reviews on Cancer* 2014, *184.1*, 75-87.

181. Sharifi-Mood N, Koplik J, Maldarelli C. Diffusiophoretic self-propulsion of colloids driven by a surface reaction: the sub-micron particle regime for exponential and van der Waals interactions[J]. Physics of Fluids (1994-present), 2013, 25(1): 012001.

182. Chen X, Shojaei-Zadeh S, Gilchrist M L, et al. A lipobead microarray assembled by particle entrapment in a microfluidic obstacle course and used for the display of cell membrane receptors[J]. Lab on a Chip, 2013, 13(15): 3041-3060.

183. Halverson J D, Maldarelli C, Couzis A, et al. Wetting of hydrophobic substrates by nanodroplets of aqueous trisiloxane and alkyl polyethoxylate surfactant solutions[J]. Chemical Engineering Science, 2009, 64(22): 4657-4667.

184. Halverson J D, Maldarelli C, Couzis A, et al. A molecular dynamics study of the motion of a nanodroplet of pure liquid on a wetting gradient[J]. The Journal of chemical physics, 2008, 129(16): 164708.

185. Davis, J.M. & Pozrikidis, C. Self-sustained oscillations in blood flow through a honeycomb capillary network. *Bull. Math. Biol*. 2014,76, 2217--2237.

186. Jeong J H, Sugii Y, Minamiyama M, et al. Measurement of RBC deformation and velocity in capillaries in vivo. Microvascular research, 2006, 71(3): 212-217.